3-2002

Development of a TM:HO:YLF-Laser-Pumped Orientation-Patterned Gallium Arsenide Optical Parametric Oscillator

Michael D. Harm

AFIT/GEO/ENP/02-01

DEVELOPMENT OF A TM:HO:YLF-LASER-PUMPED ORIENTATION-PATTERNED GALLIUM ARSENIDE OPTICAL PARAMETRIC OSCILLATOR

THESIS

Michael D. Harm, Captain, USAF

AFIT/GEO/ENP/02-01

DEPARTMENT OF THE AIR FORCE
AIR UNIVERSITY

AIR FORCE INSTITUTE OF TECHNOLOGY

Wright-Patterson Air Force Base, Ohio

The views expressed in this thesis are those of the author and do not reflect the official policy or position of the United States Air Force, Department of Defense, or the U. S. Government.

AFIT/GEO/ENP/02-01

DEVELOPMENT OF A TM:HO:YLF-LASER-PUMPED ORIENTATION-PATTERNED GALLIUM ARSENIDE OPTICAL PARAMETRIC OSCILLATOR

THESIS

Presented to the Faculty

Department of Engineering Physics

Graduate School of Engineering and Management

Air Force Institute of Technology

Air University

Air Education and Training Command

in Partial Fulfillment of the Requirements for the

Degree of Master of Science in Electrical Engineering

Michael D. Harm, BS

Captain, USAF

March 2002

AFIT/GEO/ENP/02-01

DEVELOPMENT OF A TM:HO:YLF-LASER-PUMPED ORIENTATION-PATTERNED GALLIUM ARSENIDE OPTICAL PARAMETRIC OSCILLATOR

Michael D. Harm, BS
Captain, USAF

Approved:

Won B. Roh (Chairman)	14 Mar 02 date
Kenneth L. Schepler (Member)	14 Mar 02 date
Peter E. Powers (Member)	14 Mar 02 date

Acknowledgments

In the course of any scientific endeavor, there are inevitably times when things do not turn out as one had hoped. Such was the case with this research. Although I was disappointed in the lack of results, I know that my efforts were not in vain. Others will come after me to continue research in nonlinear applications of gallium arsenide and this document will hopefully serve as a roadmap of what to consider and what not to do in future experiments.

Despite the lack of desired results, I learned a tremendous amount during this research and have many to thank for it. I am appreciative of the support and encouragement I received from the members of my thesis committee. Dr. Won Roh, my advisor, gave me wide latitude to pursue this topic with minimal oversight. In the lab, my host, Dr. Ken Schepler, gave me a place to work and always had ready answers to my "basic physics questions". Also, I am indebted to Dr. Peter Powers for allowing me to invade his laboratory at the University of Dayton to use his OPG/OPA laser when my project ground to a halt with my own laser.

I am also grateful for the many thoughtful discussions of my research with Dr. Rita Peterson, who always seemed to know when I needed some advice. I also owe an enormous debt to Captain Jason McKay for his continuous support and friendship in and out of the lab. His experience with the equipment and knowledge of experimental techniques saved me countless pieces of broken equipment and hours of wasted time.

On the domestic front, my academic accomplishments would simply not have been possible without the unwavering support of my wife and children. They have endured many late nights and weekends as a single-parent family unit as I toiled away in

the bowels of AFIT. My children have tolerated many hours of "Ssshhh! Daddy's doing his school work!" and I am looking forward to getting to know them again. Finally, as a patient and loving partner, my wife has no equal. I am grateful to a benevolent universe for every day that we are together.

Table of Contents

List of Figures

List of Tables

Abstract

Coherent optical sources in the mid-infrared region (mid-IR) are important fundamental tools for infrared countermeasures and battlefield remote sensing. Nonlinear optical effects can be applied to convert existing near-IR laser sources to radiate in the mid-IR. This research focused on achieving such a conversion with a quasi-phase matched optical parametric oscillators using orientation-patterned gallium arsenide (OPGaAs), a material that can be quasi-phased matched by periodically reversing the crystal structure during the epitaxial growth process. Although non-linear optical conversion was not ultimately achieved during this research, many valuable lessons were learned from working with this material. This thesis reviews the theory of nonlinear optics and explores the importance of accurate refractive index measurements to proper structure design. The details of four nonlinear optical experiments are presented recommendations are offered for the design of future OPGaAs crystals. Recommendations are also made for improved experimental techniques.

DEVELOPMENT OF A TM:HO:YLF-LASER-PUMPED ORIENTATION-PATTERNED GALLIUM ARSENIDE OPTICAL PARAMETRIC OSCILLATOR

I. Introduction

The U. S. Air Force has a critical need for high-power optical sources in the mid-infrared (IR) portion of the electromagnetic spectrum. Activities such as IR countermeasures and battlefield remote sensing require the ability to project tunable IR energy in the 3- to 5-μm wavelength range [27, 32, 42]. Although lasers are ideally suited to the task of projecting such energy, few materials exist with naturally tunable laser transitions in this region. Since the mid-1960's, nonlinear optical techniques have been used to shift existing laser frequencies into this important spectral region [20]. Optical parametric oscillators (OPO) are a class of nonlinear optical devices that permit wavelength shifting and are particularly useful because they split the photons of a existing laser, called the pump, into two other photons at longer wavelengths. In addition, the output of an OPO is usually tunable across a much wider spectrum than traditional lasers. However, like traditional laser devices, nonlinear optical devices are limited by the properties of available materials.

Previous Efforts

Harris listed some of the desirable qualities for materials to be used in nonlinear devices, particularly optical parametric oscillators [23:102]. Among these are high nonlinear susceptibility, phase "match-ability," high transparency and high damage limits. Although many nonlinear materials have been discovered, few have all of these

qualities in the mid-IR region. Three of the leading materials are reviewed here to highlight their strengths and weaknesses. Choy & Byer is recommended for a more detailed review of a wide array of nonlinear materials [12].

The first two substances are the chalcopyrites zinc germanium phosphide (ZGP) and silver gallium selenide ($AgGaSe_2$) [45]. These crystals are blessed with large nonlinear susceptibilities and natural birefringence [14, 52, 51]. However, each has its limitations. ZGP begins to lose transparency above 8-μm, limiting its spectral range. $AgGaSe_2$, while transparent through 12-μm, has a low thermal conductivity; maximum power throughput is limited by thermal lensing [9, 8, 36, 57]. Furthermore, because both materials are phase matched through natural birefringence, they must be pumped at precise polarization orientations and crystal angles to reach specific wavelengths. This limits their useful length through a condition called Poynting vector walk off. Walk off is a phenomenon in which the beams separate from each other as they propagate through the nonlinear medium [55:1010].

Another significant nonlinear material is lithium niobate ($LiNbO_3$), the material used to demonstrate the first OPO [20]. $LiNbO_3$ is ferromagnetic, meaning its crystal structure can be changed by applying large voltages across thin wafers. When performed correctly, the polarity of the crystal structure reverses periodically and can be artificially or "quasi"-phase matched [35]. Quasi-phase matching allows one to design the nonlinear output to a specific wavelength without angle tuning. Many $LiNbO_3$ devices have been fabricated to achieve easy tunability and increased power [7, 40]. However, this material begins to absorb radiation beyond 4-μm and cannot efficiently transmit high-power output in the mid-IR.

Promise of Gallium Arsenide

Another material, gallium arsenide (GaAs), is an excellent candidate for mid-IR nonlinear operation. GaAs has a wide transparency range from 1 to 15-μm and, with a high thermal conductivity coefficient (0.5 W-cm^{-1}-K^{-1}), has a superior resistance to damage from high laser power levels [53:7-23]. Furthermore, GaAs has a very large nonlinear coefficient, although sources vary on the exact value [12:181-2, 29:1610]. Roberts' work, the most recently published compilation of nonlinear material properties, listed GaAs's coefficient at 86 pm/V, the value used in this research [43:2068]. GaAs is also a well known and widely available material commonly used in the electronics industry [25:183]. Its only shortcomings for nonlinear applications are its lack of both birefringence and ferromagnetism. However, several techniques have been developed to overcome these limitations through other forms of quasi-phase matching.

The first attempts to quasi-phase match GaAs used thin plates cut from a single wafer [34, 50, 48]. The plates were highly polished on both sides and placed in a stack with every other plate rotated to reverse the crystal structure, as in PPLN. Thompson, et al, performed high power second harmonic generation (SHG) with a CO_2 laser with plates of high-resistivity Cr-doped GaAs. The 101±5-μm-thick plates were mounted in a precision jig at Brewster's angle to minimize reflection losses. Surface damage was noted to be about 0.3 J/cm^2 in a 3-ns pulse. Transmission loss at 10.4-μm was 0.55-dB for a stack of 19 plates, a loss coefficient of about 0.6-cm^{-1}. Power conversion efficiency for this single-pass device operating through 1.9-mm of GaAs was 2.7% for a 20 MW/cm^2 pulse. Total energy output was less than 180-μJ/pulse. This technique successfully demonstrated the feasibility of quasi-phase matching in GaAs, but the losses

associated with the numerous air interfaces of the stacked plates were too high for successful operation of an OPO.

To overcome the high scattering losses, Gordon, et al, joined a stack of GaAs plates by diffusion bonding [22:1942]. Gordon, and later, Zheng, used undoped and lightly doped GaAs wafers that were diced into 1-cm^2 squares and stacked, with every other wafer rotated 180° [56:1440]. The stack was then heated to 600° C while under pressure for 4 hours to diffusion bond the wafers together. The optical losses from this technique were 0.3-cm^{-1}, which was twice as good as the Brewster angle method of Thompson, et al [55:1011]. Power conversion was measured at 0.7% for a difference frequency generation (DFG) experiment mixing 4.78-μm and 6.75-μm laser inputs to produce a 16.6-μm idler beam. Lallier, et al, reported a similar experiment with a 1.95-μm-pump, 2.34-μm-signal, and 11.35-μm-idler combination aimed through a 45-plate stack. Although the diffusion bonding technique greatly improved the transmittance of physically manipulated GaAs stacks, all of the authors noted the hazard of working with the thin plates needed for quasi-phase matching [55;1012].

Two other approaches to quasi-phase matching in GaAs were not any more successful than the diffusion bonding method in lowering optical losses. Komine demonstrated SHG by bouncing a CO_2 laser beam along a slab of GaAs using total internal reflection [26]. Measured losses in the vicinity of 10-μm were about 20%, with an energy conversion efficiency of approximately 1%. Bravetti, et al, reported frequency conversion in a waveguide created by alternating different refractive-index layers of GaAs and aluminum oxide [6]. In this type of phase matching, called form birefringence, the incident laser beams experience different refractive indices if they are polarized

perpendicular to the layers than if parallel. While the experiment successfully generated a 5.3-μm idler beam from 1-μm pump and 1.32-μm signal lasers, losses ranged from 1.8- to 50-cm^{-1} at 5.3-μm. In summary, many techniques have been developed to access the strong nonlinearity of GaAs but almost all of them have proven too lossy to work well in an OPO.

New Growth Technique - OPGaAs

Orientation-patterned GaAs (OPGaAs) was developed in 1999 as an alternative to physically manipulating the crystal domains. Ebert, et al, created a process to grow two layers of GaAs out of phase with each other [13]. The key was to deposit a thin layer (30 angstroms) of germanium atop the first layer before laying down the second GaAs layer (see Figure 1). Ebert, et al, and Koh, et al, observed that the crystal orientation of the second GaAs layer could be reversed by adjusting the temperature of the growth process [25]. Next, a periodic structure was photolithographically-etched through the top GaAs and germanium layers to the underlying reversed or "antiphase" GaAs layer. This template then underwent molecular beam epitaxy to regrow the underlying GaAs layer up through the germanium layer [13:191]. The resulting surface, now periodic in crystal orientation, underwent a final hydride vapor phase epitaxy growth step, extending the height of the periodic structure 100's of μms. The OPGaAs proved optically pure, as the antiphase domains maintained their crystal orientations during the vertical growth process. With loss coefficients as low as 0.025-cm^{-1}, Eyres, et al, demonstrated SHG in 2000, followed by Levi, et al with DFG in 2001 [15:313, 31:21-1, 37:138]. Furthermore, by 2001, the OPGaAs could be grown to thicknesses of 500-μm without significant loss

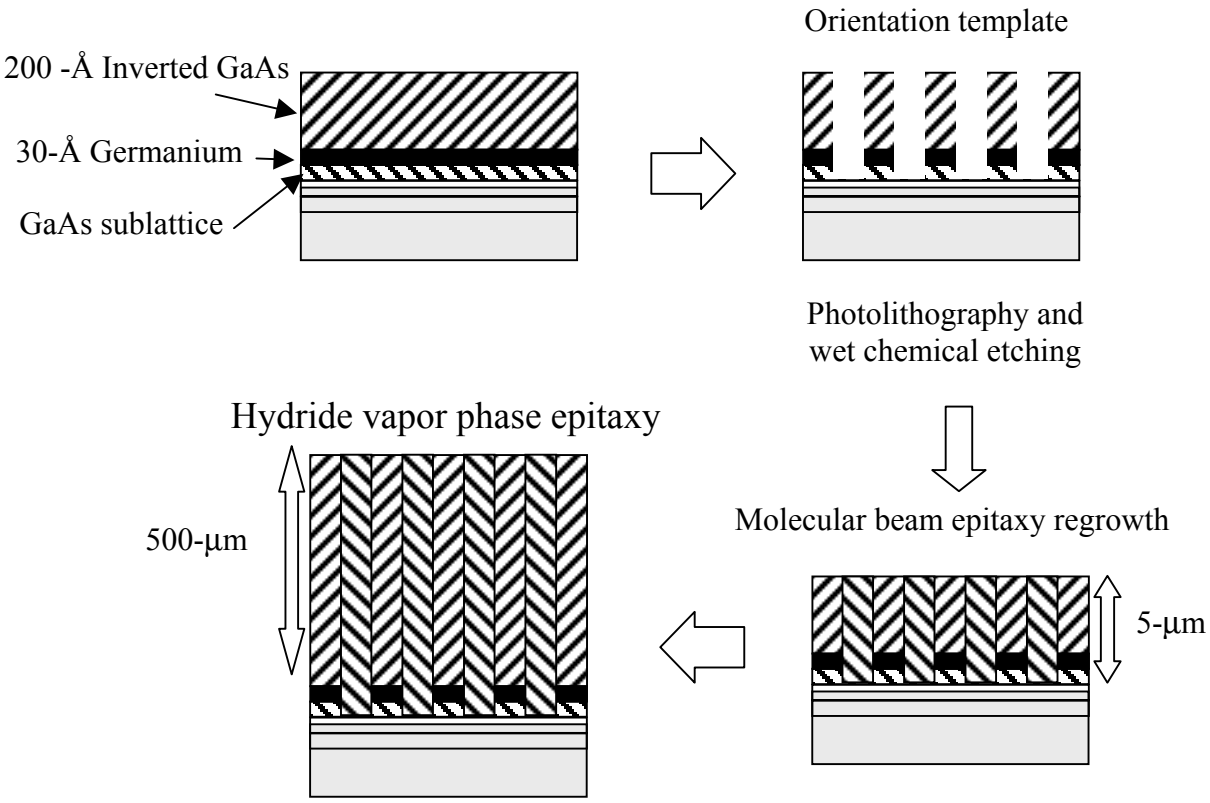

Figure 1. OPGaAs growth stages.

of periodicity [38]. This is the same thickness at which periodically-poled lithium niobate first became useful for nonlinear interactions. AFRL/SNJW and AFIT/ENP obtained two OPGaAs samples from Stanford University for a collaborative attempt to demonstrate the first OPO with GaAs. That goal became the core of this research effort.

Preview

Despite their long history, OPOs can still be difficult to operate, especially with a new material such as OPGaAs. This research effort did not achieve OPO operation in the two OPGaAs samples. However, many valuable lessons were learned that will benefit future research. Chapter II of this thesis will review the theory behind nonlinear optics

and explore the importance of accurate refractive index measurements to proper structure design. Chapter III presents the details of four nonlinear optical experiments and reviews lessons learned from them. The final chapter offers recommendations for the most suitable formulations for GaAs refractive index and outlines directions for continued research with both the current and future OPGaAs samples.

II. Theory

Quasi-phase Matching

The fundamental equations governing nonlinear optics and quasi-phase matching are nearly forty years old and have been thoroughly reviewed in a number of articles and textbooks. Rather than deriving them in detail here, this treatment will point out their fundamental origins and present the solutions relevant to quasi-phase matching, following the example of Gonzalez [21:4-9]. The interested reader can consult Yariv and Yeh [54:516] or excellent treatments by Harris [23], Byer [10,11], or Myers, et al, [35] for more detail. This treatment will begin with the equations fundamental to traditional phase matching techniques and then present the derivations tailored for OPOs.

Second-order parametric processes require the interaction of three photons of varying energies. The highest-energy photons form the pump beam, while the two lower-energy photons are the signal and idler beams. Under the proper conditions, the interaction between these three beams results in the amplification of the signal and idler at the expense of the pump. The first of these conditions is that energy must be conserved according to

$$\hbar\omega_p = \hbar\omega_s + \hbar\omega_i \qquad \textbf{(1)}$$

where $\hbar$ is Planck's constant divided by 2π, ω is the angular frequency and the p, s, and i subscripts designate the pump, signal and idler, respectively. Equation 1 states that the signal and idler photons together cannot have more energy than the pump photon. The next condition is the conservation of momentum [19:34-11, 16:2632]:

$$\hbar k_p = \hbar k_s + \hbar k_i . \tag{2}$$

Equation 2 states that the sum of the phases of the signal and idler beams must be equal to the phase of pump beam. The wave number *k* is a 3-dimensional vector defined by

$$k_j = \frac{2\pi n_j(\lambda_j)}{\lambda_j} \tag{3}$$

where the subscript j represents the pump, signal or idler beams, λ is the wavelength of the photon in a vacuum and *n* is the wavelength-dependent refractive index [10:593].

Each of the three beams must also satisfy the electromagnetic wave equation, given by:

$$\nabla^2 \vec{E} = \mu_o \frac{\partial^2}{\partial t^2}\left[\varepsilon_o (1+\chi_L)\vec{E} + \vec{P}_{NL}\right] \tag{4}$$

where $\nabla^2 \vec{E}$ is the Laplacian of the incident electric field, μ_o and ε_o are the permeability and the permittivity of free space, respectively, χ_L is the linear susceptibility and $\vec{P}_{NL}$ is the nonlinear polarization vector [21:6]. Equation 4 assumes the nonlinear material is a lossless medium and that $\vec{E}$ is a transverse plane wave for which $\nabla \cdot \vec{E} = 0$ or is very small [5:60]. $\vec{P}_{NL}$ normally contains the second-order and higher polarization terms, but an OPO involves only a second-order interaction and so only that term is considered here. $\vec{P}_{NL}$ is a vector with x-, y- and z- Cartesian components defined as

$$P_{NL-i}(\omega_1) = 2\varepsilon_o d_{ijk} E_j(\omega_2) E_k(\omega_3), \tag{5}$$

where d_{ijk} is the second-rank nonlinear coefficient tensor with units of meters per volt and *i, j,* and *k* refer to the permutations of the x, y, and z Cartesian components of the electric field vectors of two beams [54:504].

The pump, signal and idler beams can be defined as plane waves of the form:

$$\begin{aligned} E_{p-x,y} &= \frac{1}{2}\left[E_{p-x,y}(z)e^{i(k\cdot z-\omega_m t)} + c.c.\right] \\ E_{s-x,y} &= \frac{1}{2}\left[E_{p-x,y}(z)e^{i(k\cdot z-\omega_m t)} + c.c.\right] \\ E_{i-x,y} &= \frac{1}{2}\left[E_{p-x,y}(z)e^{i(k\cdot z-\omega_m t)} + c.c.\right] , \end{aligned} \tag{6}$$

where the subscripts on the *E*-terms indicate the x and y components of each pump, signal, and idler electric field. The z-direction has been chosen as the direction of propagation for simplicity. Substituting Equations 5 and 6 into Equation 4 results in a trio of coupled equations [10: 592]:

$$\begin{aligned} \frac{\partial}{\partial z}E_p + \alpha_p E_p &= i\frac{\omega_p d_{eff}}{n_p c}E_s E_i e^{-i\Delta kz} \\ \frac{\partial}{\partial z}E_s + \alpha_s E_s &= i\frac{\omega_s d_{eff}}{n_s c}E_p E_i^* e^{-i\Delta kz} \\ \frac{\partial}{\partial z}E_i + \alpha_i E_i &= i\frac{\omega_i d_{eff}}{n_i c}E_p E_s^* e^{-i\Delta kz} . \end{aligned} \tag{7}$$

Here, α_j is the round trip electric field loss and n_j is the refractive index of the material at the each wavelength. Δk is the wave vector mismatch defined by

$$\Delta k = k_p - k_s - k_i \tag{8}$$

which is merely a restatement of Equation 2. The d_{eff} term is the effective nonlinear coefficient determined by the direction of propagation, the structure of the d-tensor, and the angle of the pump wave polarization vector. Calculations presented in Appendix A show that d_{eff} has a maximum of $0.74 \cdot d_{14}$ for OPGaAs when the pump, signal and idler beams are propagating along the [0 1 1] direction and are polarized at 54.7° from the [0 0 1] direction, which agrees with Zheng, et al [55:1011].

Equations 1 through 7 apply to traditional birefringently phase matched materials. GaAs is isotropic and therefore must employ quasi-phase matching to create practical energy conversion. If a nonlinear material is not phase matched, the energy will flow sinusoidally back and forth between the pump and the signal and idler beams [11:562]. However, if the sign of the effective nonlinear coefficient could be reversed every time the exponential term changes sign (i.e. when $\Delta kz = m\pi$, with m being an integer), then the nonlinear interaction would continue to grow. Figure 2 compares the nonlinear

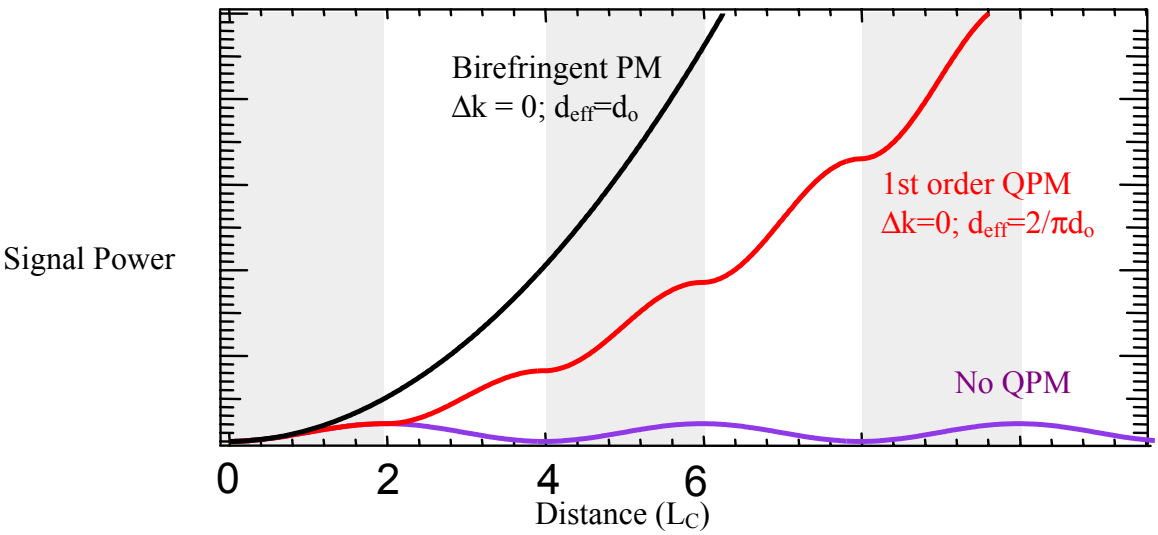

Figure 2. Quasi-phase matching versus birefringent phase matching. L_C is the length along the direction of propagation. For quasi-phase matched interactions, the nonlinear coefficient, d, is reduced by a factor of $2/\pi$. [44]

interaction for birefringently phase matched and quasi-phase matched materials. The reversal distances are called coherence lengths and are defined by

$$\ell_c = \frac{\pi}{k_p - k_s - k_i} \tag{9}$$

A structure with a nonlinear coefficient modulated every other coherence length is a spatial grating with a period $\Lambda = 2\ell_c$. A Fourier series representation of the periodic structure produces a grating vector in phase space defined by

$$k_g = \frac{2\pi}{\Lambda} \tag{10}$$

which allows Equation 8 to be rewritten as

$$\Delta k_{QPM} = k_p - k_s - k_i - k_g. \tag{11}$$

Finally, the gain equation for an optical parametric oscillator can be presented. In the presence of a strong pump wave and a single photon per signal mode, the single pass power gain is [11:564]

$$G_s(L) = \frac{|E_s(L)|^2}{|E_s(0)|^2} - 1 = \frac{2\omega_s \omega_i d_{eff}^2 I_p}{n_s n_i n_p \varepsilon_o c^3} L^2 \frac{\sin^2\left(\Delta k_{QPM} \cdot L\right)}{\left(\Delta k_{QPM} \cdot L\right)^2} \tag{12}$$

where L is the overall length of the quasi-phase matched portion of the nonlinear crystal, I_p is the pump beam intensity at the beam waist in units of W/m^2, and the limit of low gain has been assumed. The threshold intensity for a singly resonant OPO is derived as

$$I_{th} = \frac{n_s n_i n_p \varepsilon_o^3 c^3}{\omega_s \omega_i d_{eff}^2 L^2} \frac{\left(1 - R_s^2 e^{-2\alpha_s L}\right)}{\left(R_s^2 e^{-2\alpha_s L}\right)} \tag{13}$$

where the term $R_s^2 e^{-2\alpha_s L}$ represents the OPO cavity round-trip power loss for OPO mirrors with reflectivity R_s and for a nonlinear material with loss coefficient α_s at the signal wavelength [54].

All of the previous equations have assumed plane waves interacting within the nonlinear material. However, real beams have approximately Gaussian profiles and diverge at different rates. The pump wave described above will be focused into the nonlinear material and will not maintain a uniform cross-section over the length of the crystal (see Figure 3). Furthermore, if the resonated signal beam is not confocal with the pump, their volumes will not overlap, decreasing the efficiency with which the pump amplifies the oscillating signal photons. This volume mismatch would act as an additional round-trip loss, raising the threshold determined from Equation 13. On the other hand, Boyd and Kleinman showed that if the nonlinear crystal length L is less than 0.4 times the confocal parameter, given by

$$b = 2z_o = \frac{2\pi n \omega_o^2}{\lambda}, \tag{14}$$

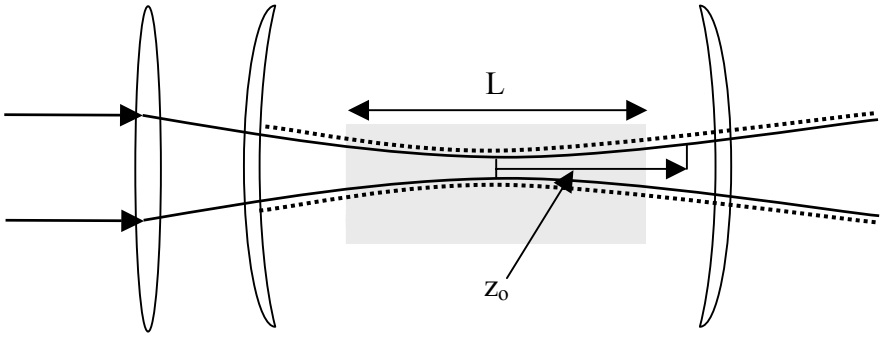

Figure 3. Confocal region of OPO crystal. When $L<<2z_o$, the cross-sectional areas of the beams remain constant and can be considered plane waves. Z_o is the Rayleigh range.

the beam cross sections will remain essentially constant within the crystal and the effects of focusing can be ignored [4:48]. This is known as the weak focusing limit. Furthermore, if the OPO cavity is designed such that the signal beam converges to the same size waist at the same position as the pump beam, then the volume mismatch can be ignored as well.

Sellmeier Equations

The primary advantage of quasi-phase matching is the ability to design a phase-matched nonlinear interaction at desired wavelengths rather than relying on naturally-occurring interactions. This is accomplished by specifying the pump and signal (or pump and idler) wavelengths, and applying the energy and momentum conservation relations of Equations 1 and 11. A key design parameter, however, is the accuracy to which the refractive index is known for the wavelengths of interest. Equation 12 shows that the power gain is proportional to sinc^2, a function that reaches its peak when $\Delta kL=0$ (see Figure 4). However, sinc^2 decays dramatically as Δk moves away from zero, reaching its first null at $\Delta kL=\pm\pi$. The peaks beyond $\pm\pi$ are so small as to be practically negligible. If L is on the order of a few centimeters (typical for an OPO), the grating vector must reduce the difference between the first three terms of Equation 11 to a number with an order of magnitude of about 10^2-m^{-1}. Now, consider Equation 11 rewritten in the following form:

$$\Delta k_{QPM} = \frac{n_p(\lambda_p)}{\lambda_p} - \frac{n_s(\lambda_s)}{\lambda_s} - \frac{n_i(\lambda_i)}{\lambda_i} - \frac{1}{\Lambda_g} = 0 . \qquad \textbf{(15)}$$

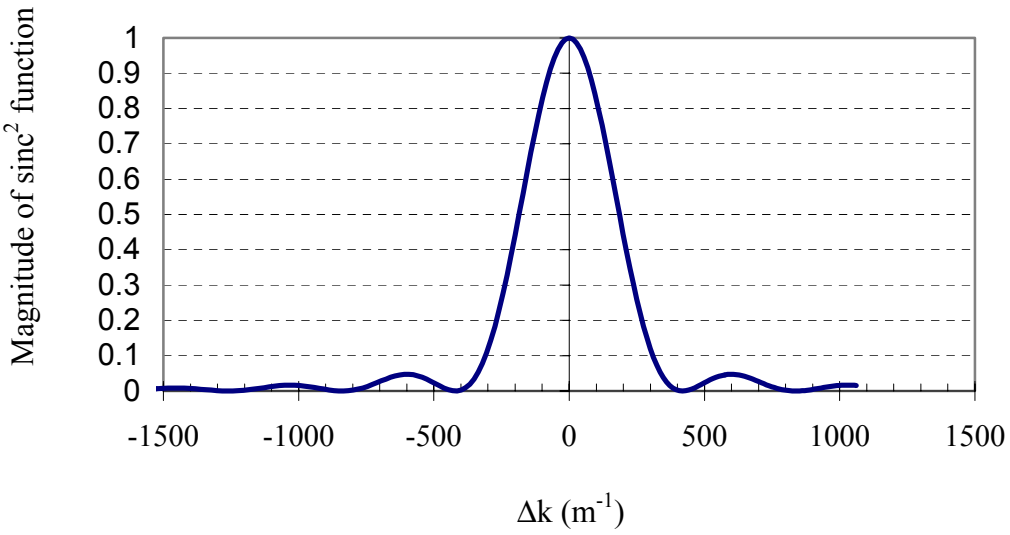

Figure 4. Sinc^2 function.

In the mid-IR, the units of the wavelengths are microns, so the first three terms are on the order of 10^6-m^{-1}. Consequently, a refractive index error of as little as 10^{-4} at any of the three wavelengths would be magnified sufficiently to spoil phase matching. Additionally, this points to the need to specify the grating period (usually in the tens of microns) to the same level of precision. Indeed, Fejer, et al, derived the following formula for the FWHM acceptance width of the grating period under the sinc^2 function [16:2635]:

$$\delta\Lambda = \frac{3.55m\ell_c^2}{L} \tag{16}$$

where m is the duty cycle of the periodic structure. For a 1-cm crystal with a 30-μm coherence length, the FWHM deviation in each coherence length is only 0.07-μm. Figure 5 shows the loss of quasi-phase matching in an OPGaAs structure as the design coherence length changes by less 1-μm. The need for accurate refractive index

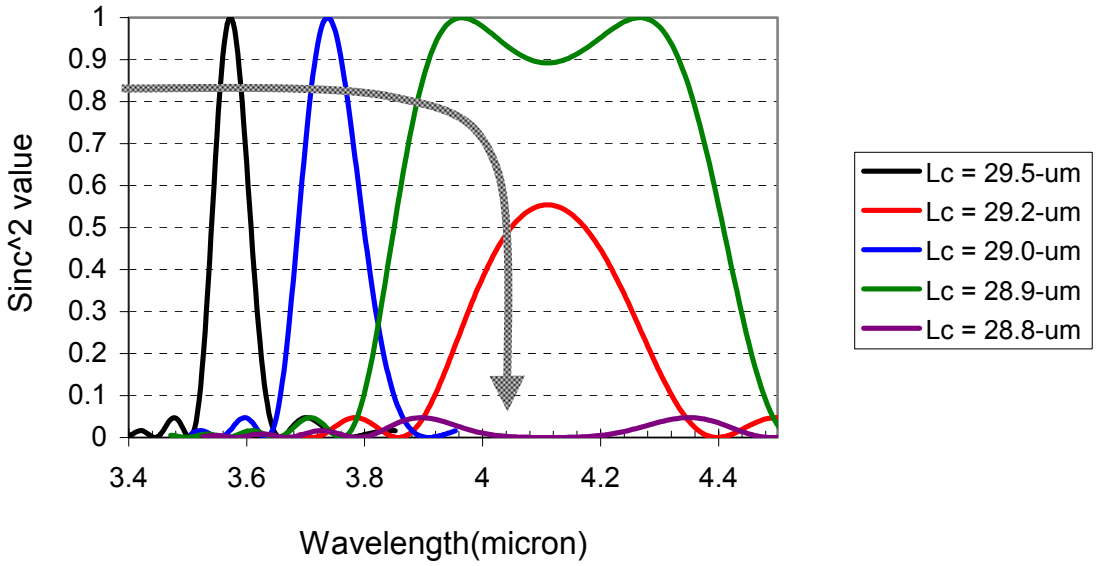

Figure 5. Effect of small changes to coherence length on OPO gain. This graph presents the predicted strength of a signal beam from an OPGaAs OPO designed with a variety of coherence lengths for a 2.055-μm pump beam. As the coherence length, Lc, decreases, the strength of the nonlinear interaction rapidly falls to zero.

formulations, known as Sellmeier equations, is clear. However, despite the maturity of this widely used semiconductor, the refractive index is not well modeled in the mid-IR.

Choy and Byer noted 25 years ago that the index of refraction of GaAs was not known accurately enough, and a search of the literature before and since failed to contradict them [12:177]. Formulations abound for the refractive index of GaAs, but few of them agree. In 1996, Tanguy cited more than 25 models and experimental measurements [49:1746], but most of them concentrated on modeling the refractive index around the high-absorption regions of GaAs, such as the bandgap or the phonon-absorption points in the far infrared, ignoring the transparency region in the mid-IR. Furthermore, since GaAs is of considerable interest as a semiconductor, many different doping levels were considered among the experimental samples, making it impossible to directly compare the different results. In most cases, the authors happily reported curve

fittings to within two or three significant digits, which is insufficient for quasi-phase matching purposes.

Figure 6 presents seven representative formulations for comparison. The oldest, by Barcus, was based on a least-squares fit to reflection angle measurements [1]. Unfortunately, his experiment collected data mostly in the 10-µm region with just a single data point at 2-µm. Seraphin and Bennet, Blakemore, and Feldman and Waxler based their Sellmeier equations on a host of historical data, including that of Marple [3, 18, 33, 47]. Unfortunately, Marple's investigation, widely referenced as an accurate measurement of GaAs refractive index, did not extend into the mid-IR either, stopping at 1.7-µm. Sell, et al and Tanguy investigated GaAs refractive index around the band gap

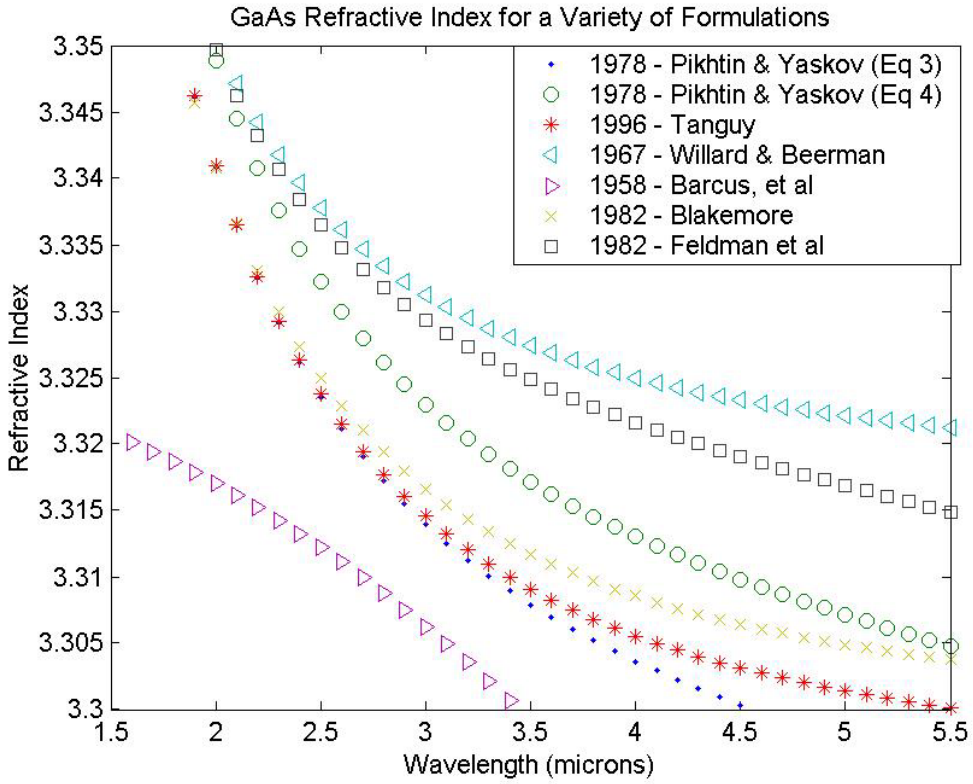

Figure 6. GaAs refractive index formulations.

(about 0.870=µm, depending on doping), with Tanguy's model being the most thorough treatment of possible absorption points through much of the spectrum [46]. Regrettably, Tanguy's formulation neglected Sellmeier equation terms needed to achieve precision better than 0.002 [49:1748]. Finally, Pikhtin and Yas'kov produced a pair of formulations based on their own mid-IR data that are widely considered the benchmark for GaAs refractive index [39]. These were labeled Equations 3 and 4 in their paper, and are referred to here as Pikhtin3 and Pikhtin4. Although they did measure refractive index in the mid-IR, Pikhtin and Yas'kov collected their data at 105° K, so the applicability of their equations to room temperature operations is questionable.

Five of these Sellmeier formulations were selected to calculate the required grating period of an OPGaAs OPO pumped by a 2.055-µm laser. The results in Figure 7

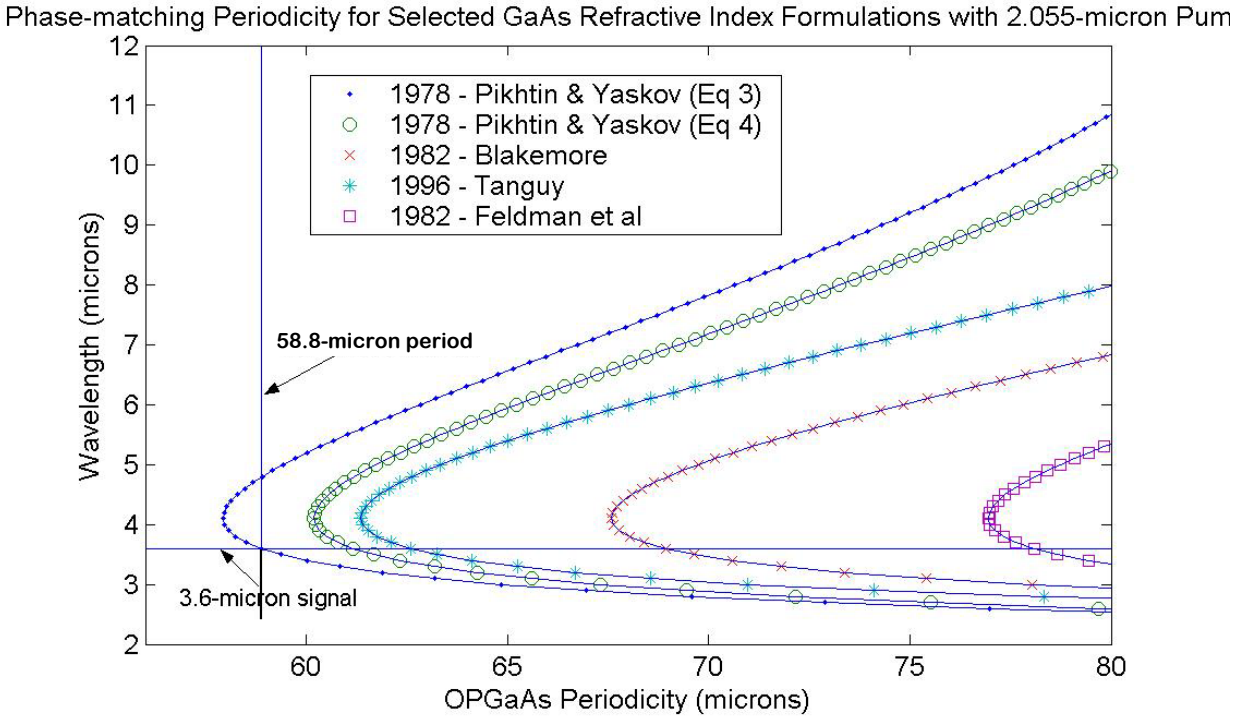

Figure 7. Phase matched periodicities for a 2.055-µm pump laser in OPGaAs.

illustrate the dramatic differences among them. Each curve in the figure represents quasi-phase-matched wavelengths calculated to conserve both momentum and energy for the individual OPGaAs periods specified along the horizontal axis. Here, one sees that the seemingly small changes among the formulations result in dramatic changes to the required periodicity. One also notes that for each equation, there is a minimum periodicity below which phase matching cannot be satisfied (also seen in Figure 5).

Unfortunately, no other research has attempted to design a quasi-phase matched OPGaAs structure operating squarely in the 2-5-μm region. Levi, et al, and Koh achieved phase matching at near-IR wavelengths using Pikhtin4 [25, 31, 17]. Lallier's and Zheng's successful DFG experiments also referenced Pikhtin and Yas'kov's paper for frequencies that bracketed the 2-5-μm range, but did not specify which formulation they used. Ultimately, collaborating researchers at Stanford University designed the OPGaAs samples for this research with Pikhtin3. In retrospect, this was not the shrewdest choice, given the uncertainty among the GaAs Sellmeier equations and the extremeness of the Pikhtin3 solution [17].

OPGaAs Samples

The OPGaAs structures for this research were designed to operate purely in the 2-5-μm region of the mid-IR. A previously developed laser operating at 2.055-μm was specified as the pump laser. The signal and idler outputs were designed for 3.6- and 4.78-μm respectively to take advantage of two mid-IR transmission windows in the atmospheric absorption spectrum commonly used for IR countermeasures and remote sensing [53:5-88-9]. Using Pikhtin3, the required periodicity for these wavelengths was

58.8-μm as calculated from Equation 15. The Stanford University research group prepared the two samples using the all-epitaxial growth technique discussed earlier. Both samples were approximately 5-mm wide and 1-mm thick, with only the top 0.5-mm available for phase-matching experiments. Sample 1 was 19-mm long, but only 14-mm was orientation-patterned. Sample 2 was 14-mm long, of which 10-mm was orientation-patterned (see Figure 8). Periodicity was measured to be 58.8-μm, ± 0.1-μm, with a Zeiss microscope at 80-times magnification. The two samples were AR coated on both end faces to be highly transmissive at the pump, signal, and idler frequencies.

The crystals were examined with an IR camera and both displayed poor transparency. A tightly focused, low power 2.052-μm laser beam was directed into each sample, with a Hamamatsu IR camera imaging the entrance and exit faces. Both samples showed numerous optical aberrations and anomalies along the height and width of the crystal. In particular, Sample 1 displayed a strong horizontal band of absorption across the middle of the transparent region. This band was not an interference fringe, being unchanged in size when the angle of the crystal was adjusted. In Sample 2, a few clear regions less than 100-μm in diameter were identified as marginally acceptable for an OPO. Unfortunately, no camera images were recorded before the crystals were damaged, so no IR images are presented here.

Absorption at 2.052-μm was measured by recording the incident and transmitted power with a Newport 1845 thermopile. Reflected energy was assumed to be negligible. A 10% reduction in power was noted for Sample 2, which corresponds to an absorption coefficient, α, of 0.075-cm^{-1}. Absorption in Sample 1 was not measured. This value is

comparable to the best absorption coefficients reported from the diffusion bonding technique [55:1010, 29:1609,]. However, the numerous optical aberrations noted earlier could be expected to offset the advantages of this promisingly low absorption loss by spoiling the phase-front of the resonating signal beam.

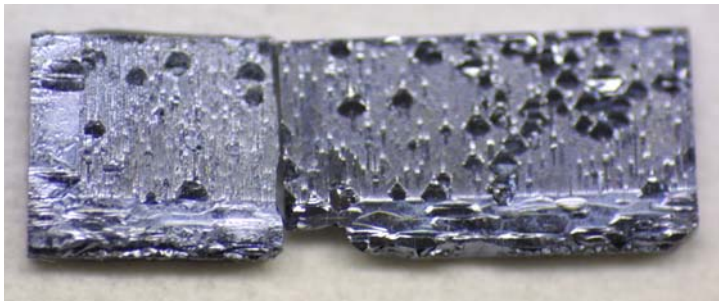

a

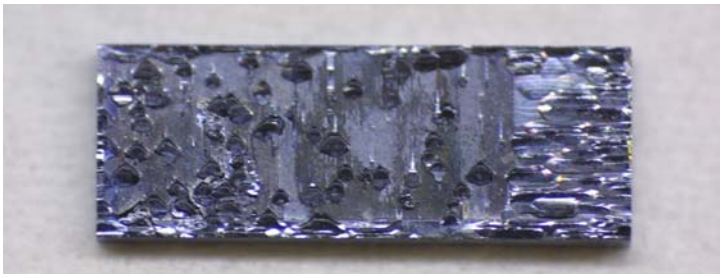

b

c

Figure 8. OPGaAs experimental samples. a) Sample 1 – Length: 19-mm (broken after a fatal encounter with the floor). b) Sample 2 – Length: 14-mm (only 10-mm were orientation-patterned). c) Face of sample 2 polished shown end-on with a fine-tip pen for a sense of scale. The face is 1-mm thick by 5-mm wide, but only the top 0.5-mm was orientation-patterned.

III. Experiments

OPO Experiment

Background. The OPGaAs samples discussed in the previous section were designed for a 2.055-μm-laser-pumped OPO. This section details the experimental equipment, including the pump laser, which actually emitted at 2.052-μm, and the OPO cavity optics. The procedures and power settings are also presented. This experiment was not successful, however, and the final portion of this section discusses several possible explanations for the negative results.

2.052-μm Pump Laser. The starting point of the OPGaAs OPO was a laser-diode-pumped, thulium-holmium-doped yttrium-lithium-fluoride (Tm:Ho:YLF) 2.052-μm pump laser (see Figure 9). The laser diode was a 15-W array of continuous-wave aluminum gallium arsenide (AlGaAs) devices emitting at 792-nm (Opto Power Corp. model OPC-A015-mmm-FC) through a 1-meter optical fiber. The laser diode output was coupled through a pair of AR-coated 6-cm focal length lenses into the 5x5x5-mm^3 Tm:Ho:YLF crystal. Concentrations of Ho and Tm were 1% and 6%, respectively. The crystal was mounted on a copper cold finger in a liquid-nitrogen-cooled dewar. The side facing the laser diode (LD) was AR-coated for 792-nm, highly-reflective (HR) coated for 2.05-μm and acted as the planar end of the plano-convex 2.052-μm laser cavity. A 200-cm focal length lens reflecting 70% of the pump beam was the output coupler. The pump laser was pulsed at 1 kHz with a water-cooled acousto-optic Q-switch. A half-wave plate together with a polarizing Faraday isolator allowed for

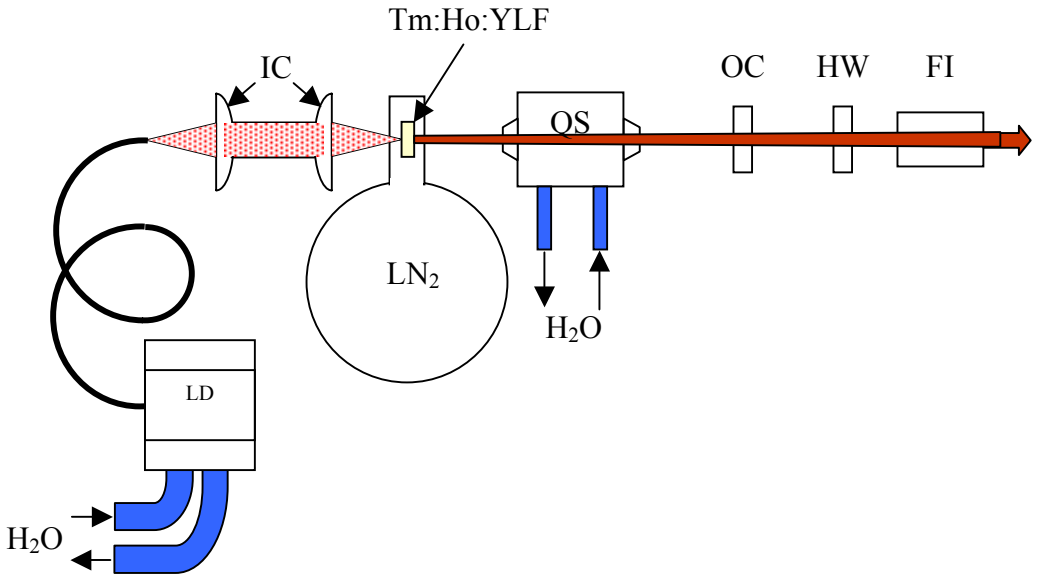

Figure 9. 2.052-µm Tm:Ho:YLF pump laser. LD – 792-µm 15-W laser diode; IC – 6-cm focal length input couplers, AR-coated for 792-µm; QS – acousto-optic water-cooled Q-switch; OC – 200-cm focal length output coupler, 70% reflective at 2.052-µm; HW – 2.05-µm half-wave plate; FI – 2.05-µm Faraday Isolator

precise control of the magnitude of the 2.052-µm laser output and selection of its polarization angle.

The pump laser ran robustly and required little adjustment once warmed up. Figure 10 displays the performance of the Tm:Ho:YLF laser as a function of LD pumping power. The pump laser demonstrated a threshold of 1.8-W of LD input with a slope efficiency of 25% above 8-W input power. Maximum Q-switched output was 2.6-W average power, or 2.6-mJ per pulse. The pulse length ranged from 100-ns FWHM at 1mJ average power to less than the 40-ns time constant of an Au:Ge detector at the maximum output. The pump laser spectral output was measured with an Acton 0.75-m monochromator (see Figure 11). A glass microscope slide inserted in the laser cavity narrowed the laser bandwidth to 0.2-nm, with a peak at 2.0524-µm, comparing favorably to that of other Tm:Ho:YLF lasers [2:2423]. The spatial qualities were also good, with

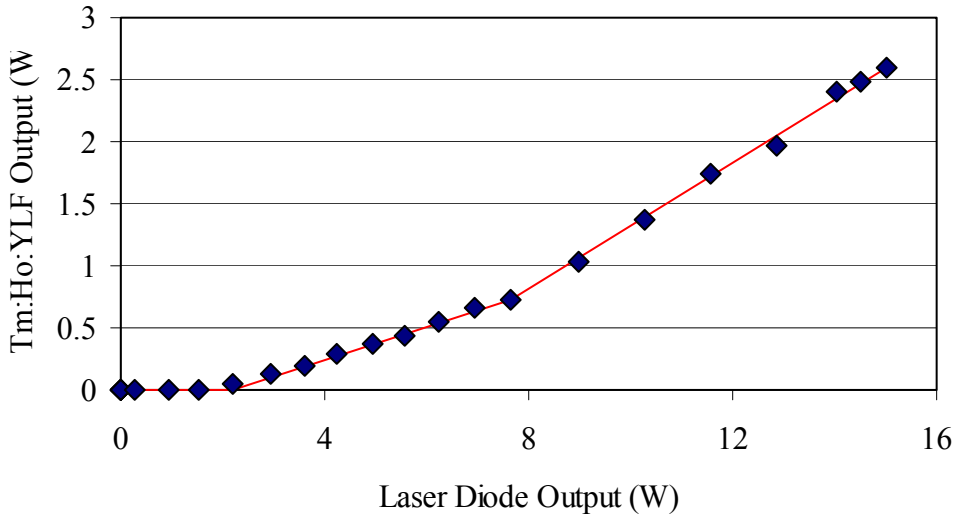

Figure 10. Tm:Ho:YLF performance. The symbols denote measured data and the solid line denotes a linear curve fit to the data. The Tm:Ho:YLF 2.052-µm output demonstrated a slope efficiency of 13% below 8-W LD input and 25% above it. The cause of the slope change at 8-W input power was not determined.

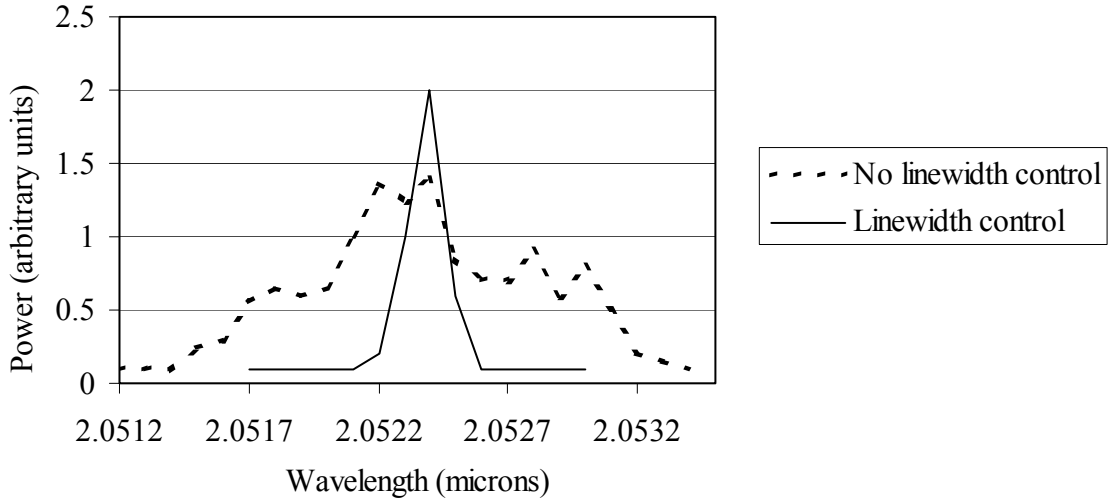

Figure 11. Spectral output of Tm:Ho:YLF laser. Laser linewidth was controlled with a microscope slide and was reduced to about 2-Å at 2.054µm.

an M^2 of about 1.5. The beam quality was observed with a Hamamatsu 2-μm IR camera and displayed a slightly elliptical gaussian intensity profile, with the long axis in the horizontal plane at a 6:5 ratio compared to the vertical. The beam was focused through an uncoated CaF_2 lens into the OPO cavity. A 20-cm focal length lens produced a 70-μm radius spot as measured with a scanning razor blade, while a 10-cm lens reduced the beam waist to 40-μm.

OPO Cavity. The singly-resonant OPO cavity was constructed from a pair of CaF_2 meniscus lenses coated to pass both the pump and idler beams while reflecting 99.9% of the signal photons between 3.3- and 3.8-μm. The OPO cavity mirrors were mode-matched to the pump beam according to Appendix B. The use of a 40-μm waist required the mirrors to be positioned near the edge of cavity stabilility for the resonator. OPO output was filtered with a pair of dichroic mirrors that rejected 99.99% of the pump energy, but reflected 60% of the signal to a Newport model 818J thermopile detector head connected to a Newport 1835J energy meter.

Procedures. The OPO cavity was aligned with the pump beam using a HeNe laser and temperature-sensitive liquid crystal paper. A microscope slide placed in the pump beam merged the HeNe and pump lasers, which were focused through the OPO mirrors onto the face of the crystal. The alignment laser reflections from both surfaces of the OPO mirror and from the OPGaAs crystal formed interference fringe patterns reflected back to the face of the HeNe laser head. Both surfaces were adjusted until the fringes were centered on the opening of the HeNe. Next, the pump beam exiting the OPO was directed onto a mirror at the far end of the optics bench. The HeNe was

adjusted to illuminate the same spot and the mirror was rotated until the pump beam reflection was centered on the HeNe laser head. With the two beams co-linearized, the second OPO mirror was placed in the beam path and aligned to the HeNe laser in a similar manner as the first. Both OPO mirrors were mounted on micro-adjustable lens holders to facilitate cavity alignment and were placed at appropriate positions for mode matching as specified in Appendix B to within 1-mm. OPO output was sought by raster-scanning the second OPO mirror. The pump beam polarization angle was adjusted using the half-wave plate. Initial OPO alignment attempts were performed with the pump beam vertically polarized in the [1 0 0] crystal direction, but attempts were also made at 45° (≈[5 7 $\bar{7}$]) and 90° ([0 1 $\bar{1}$]) angles from the vertical.

Results. No OPO interaction was observed for any configuration or power setting. The first OPO alignment attempts focused the pump beam with a 20-cm focal length CaF_2 lens to a 70-μm radius beam waist through the 10-cm focal length OPO mirrors. The pump beam delivered up to 200-μJ in 100-ns pulses. After noting the previously mentioned aberrations in both crystals, the smaller 40-μm waist was applied at power levels up to 30-μJ in 40-ns pulses. Exact measurement of the duration of these shorter pulses was limited by the 50-ns time constant of the detection equipment. A 1° wedge was observed on OPGaAs Sample 2 and the second OPO mirror was adjusted accordingly.

Damage thresholds were disappointingly low and were attributed to poor quality AR coatings on the OPGaAs samples. The coatings damaged at energy levels of 0.6-J/cm^2 in 40-ns and 1 J/cm^2 in 100-ns. Care was taken to ensure the crystal surfaces

were free from dust and smudges. Coating damage was determined by noting a decrease in pump power through the OPGaAs samples on the Newport detector. For the low power setting, the damage was observed real-time with an IR camera. The coatings were observed to damage within seconds at the energy levels specified, usually on the input face of the crystal. Burn marks on the exit face only occurred at power settings well above the noted damage thresholds (see Figure 12 b and c). To be conservative, subsequent power settings were limited to half of the damage thresholds noted above.

Discussion

There are a number of possible reasons why this OPO experiment did not succeed. The most likely reason was that OPGaAs samples were not properly quasi-phase matched for the 2.052-μm pump laser. The required periodicity for these

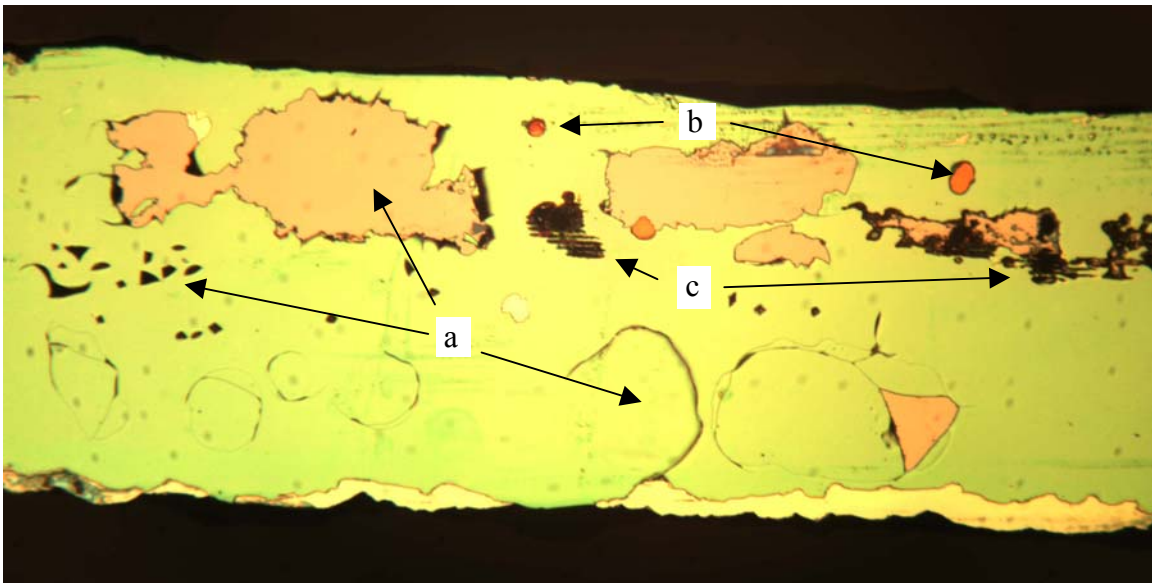

Figure 12. Laser burn and thermal stress damage to AR coating on OPGaAs Sample 1. a) Different thermal expansion rates caused the AR coating to crack and flake away. Only the outermost layer appeared to be affected. b) Damage caused by focused laser energy entering the pictured face. c) Damage caused by laser energy exiting the pictured face. Damage was noted on the exit surfaces only for high-power pump pulses.

samples was determined using Pikhtin3. However, Tanguy found that Pikhtin and Yas'kov overestimated by half an important term in their formulation [49:1748]. Unfortunately, Tanguy's research was discovered only after this series of experiments was completed. The uncertainty regarding the precise values of the refractive index and the importance of that precision could sufficiently explain the lack of results.

Besides a lack of phase matching, the OPO threshold may have been higher than initially calculated for several other reasons. First, the OPGaAs samples were so optically irregular that the pump beam was significantly distorted after just one pass. Smaller-diameter beams were able to find somewhat clearer paths through the crystals than larger beams, but such paths were few in number. Any optical distortion through the crystals would have increased the round-trip losses, thereby increasing the OPO threshold.

Second, the threshold calculation presented in Section 2 depended on an assumption of very low round-trip losses. The OPGaAs samples were far from low-loss, demonstrating round trip losses of 20%. In the presence of significant losses, the loss term in Equation 13 become

$$1 - R_s^2 e^{-2\alpha_s L} \quad \Rightarrow \quad 2\alpha_{sp} = -2\ln(R_s) + 2\alpha L\,, \tag{17}$$

where α_{sp} is the single-pass cavity loss [4]. This results in a calculated loss closer to 23%.

A third factor not considered in initial threshold calculations was the rise time required to amplify the background signal noise to the magnitude of the pump [10:612-5]. The following relation for an SRO is derived from Byer:

$$N = 1 + \frac{L_c \ln\left(P_s(t_1) / P_s(t_0)\right)}{2\tau_r c\alpha}. \qquad \textbf{(18)}$$

N is the number of times above threshold that an OPO must be pumped to reach the magnitude of the pump power in the specified rise time, τ_r. The ratio of $P_s(t_1)/P_s(t_0)$ represents the amount of gain required to amplify the signal beam from a single photon and is usually specified as 10^{12}. α represents all losses within the cavity and L_c is the effective cavity length. Setting τ_r equal to a pump pulse duration of 100-ns in a 20-cm OPO cavity gives a threshold increase of 90%, and a 40-ns pulse raises the threshold by 230% (see Figure 13).

A final parameter affecting OPO threshold was mode matching between the pump and signal beams. The beam waists used to achieve reasonable beam quality through the OPGaAs samples were very small. To mode match the signal to these small waists, the

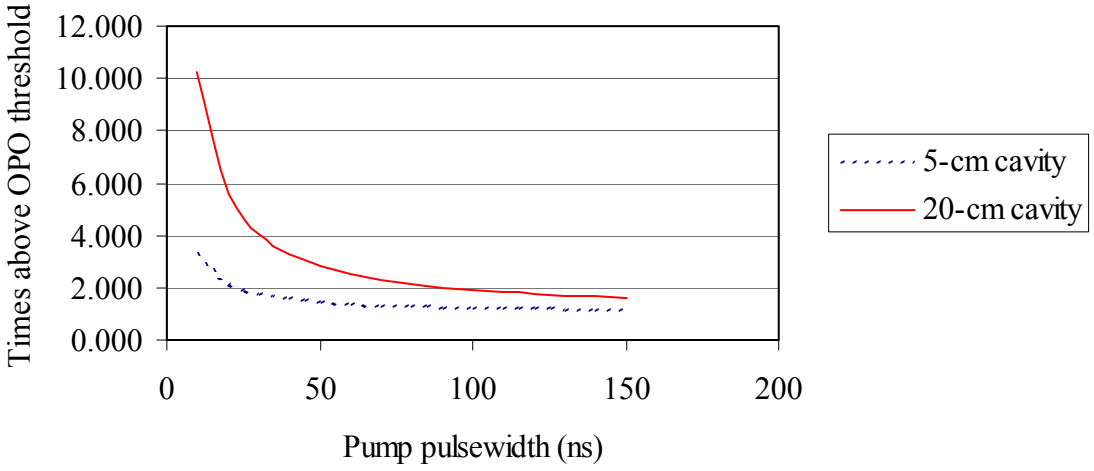

Figure 13. Effect of pump laser pulse-width on SRO threshold of an OPO cavity. Pump threshold is significantly higher for a 100-ns, the OPO must be pumped at 1.9 times the threshold calculated in Equation 13. At 40-ns, the energy requirement increases 3.3 times above threshold.

OPO mirrors had to be positioned with sub-millimeter accuracy (see Appendix B). However, experimental mirror placement accuracy was no better than ±1-mm. The cavity may not have been properly mode matched for the smaller beams, which also would have increased the OPO threshold according to the following relation: [4]

$$g_{mm} = \frac{2w_s^2}{w_s^2 + w_p^2}. \tag{19}$$

where w_s and w_p are the radii of the pump and signal beam waists and g_{mm} is a factor that reduces the gain. When combined, these loss factors change Equation 13 to

$$I_{th} = \frac{n_s n_i n_p \varepsilon_o^3 c^3}{\omega_s \omega_i d_{eff}^2 L^2} \frac{2\alpha_{sp}}{1 - 2\alpha_{sp}} \frac{N}{g_{mm}}. \tag{20}$$

The effect on OPO threshold is seen in Table 1. The OPO threshold for the 40-ns pump pulse is now predicted to occur at the power levels at which the coated surfaces began to damage. One does note, however, that the 100-ns pulse should have achieved operation

Table 1. OPO threshold with additional losses. With the additional loss factors, the threshold for a 40-ns pulse occurs at the observed damage threshold. The longer 100-ns pulse was predicted to reach threshold below the corresponding damage level.

	Threshold (J/cm^2)		
Pump Pulsewidth (ns)	Original Calculation (Equation 13)	With New Loss Terms (Equation 20)	Observed Damage Level
40	0.11	0.62	0.6
100	0.27	0.92	1.3

before burning the AR coatings, supporting the theory that the crystals were not quasi-phase matched.

Finally, one cannot dismiss the possibility of simple experimental errors to explain the negative outcome of this experiment. First, the dichroic mirrors used to filter the pump beam from the OPO output also filtered out the idler wavelength. Only about 60% of the signal beam would have been reflected into the detector. However, the OPO cavity was designed to resonate the signal beam with high reflectivity. Therefore, even if the OPO had reached threshold before the AR coatings were damaged, the signal beam would have been mostly retained within the cavity, with less than 0.06% getting to the detector. A better choice would have been to use output filters that reflected the idler wavelength. Second, the OPO cavity was mode matched to such small beam waists that the mirrors had to be adjusted to within half a milliradian of the correct alignment position. It is possible that the large, fine raster scan employed was not fine enough and that the optimal alignment point was never found.

DFG Experiment

The negative results from the OPO experiments in the previous section could be explained by deficient phase matching but there were enough questions about the experimental technique to warrant a second look with a DFG experiment. OPO configurations require precise cavity alignment to achieve operation whereas DFG interactions have no cavities. Several DFG experiments were attempted to observe nonlinear operation. This section will briefly review the theory of DFG, specify the equipment used, and discuss the results of the experiments.

Background. In a DFG interaction, two laser beams (the pump and signal) are coaligned and make a single pass through the nonlinear crystal. With proper phase matching, the signal beam is amplified at the expense of the higher-energy pump beam. Simultaneously, an idler wave is created at a wavelength that conserves energy according to Equation 1. Unlike an OPO, the signal wave does not need to resonate to build up strength, so there are no mirrors to align. Also, the idler beam does not start from noise. Instead, new idler photons are created in the same proportion as the new signal photons [54:533]. For example, the single pass power gain of OPGaAs Sample 2 was calculated to be ≈2.5. If a pump beam supplies 10-μJ per pulse at 2.052-μm and the signal beam supplies 1-μJ per pulse at 3.6-μm, then 2.5-μJ of signal photons would be produced during amplification. By the Manley-Rowe relation, the same number of photons is also produced at the 4.78-μm idler wavelength [54]. Due to the lower energy level of the idler photons, however, this would amount to 3.6/4.78, or 75%, of the amplified signal energy. Nevertheless, such a small idler beam is detectable with a liquid-nitrogen-cooled photoconductor and, if detected, would verify that the OPGaAs samples are correctly phase matched.

Procedure. The same Tm:Ho:YLF laser provided one of the two beams for this experiment. The second beam was generated by a periodically-poled lithium niobate (PPLN) optical parametric amplifier seeded with a PPLN optical parametric generator (OPG) [41]. The two crystals were pumped with a Coherent Infinity Nd:YAG laser that produced a 3.5-ns, 10-Hz beam at 1.064-μm. This output was split into two beams. The first beam was focused into a PPLN grating that produced output via OPG. The broad-band signal output of this first PPLN crystal was then narrowed through an

adjustable Fabry-Perot etalon and focused into a second PPLN crystal along with the other half of the pump beam. The narrow-band signal beam was amplified in the second crystal, which also produced narrow-band (1.2-nm FWHM bandwidth) signal and idler beams. The beam quality was adequate, with a waist of 340-μm horizontal by 300-μm vertical determined by noting the 10%-peak-power points with a scanning razor blade.

The OPG/OPA PPLN laser was tunable over a wide range of wavelengths, allowing experimentation with shorter pump wavelengths. A calculation with equation 15 showed that quasi-phase matching with the existing OPGaAs coherence lengths could be achieved if the 2.052-μm beam were mixed with a 1.734-μm pump beam. The OPG/OPA PPLN device could provide this wavelength as its signal output. In addition, the device could be tuned to generate a 3.6-μm beam as its idler, which in turn would match the phase requirements of a 2.052-μm pump beam. It was immediately observed, however, that the 1.734-μm beam was more than 90% absorbed as it passed through the OPGaAs crystal. Although GaAs is normally transparent at that wavelength, the intensity of the OPG/OPA output (about 100-kW/cm^2 in a 3.5-ns pulse) probably triggered a two-photon absorption mechanism. This huge loss demonstrated that pulsed pumping of OPGaAs was not feasible at this wavelength or lower. Consequently, this experiment was limited to the 2.052-μm and 3.6-μm beams. The power of the 3.6-μm beam at the OPGaAs crystal face was 3.5-4-μW.

The combination of these two lasers presented an intriguing challenge. The first issue was pulse timing. The 2.052-μm laser produced a 40-ns pulse Q-switched at 1kHz, while the Nd:YAG was limited to 10-Hz with a 3.5-ns pulse-width. A method had to be

developed to synchronize every 100th pump pulse with each signal pulses. Several iterations of equipment were tried, but the best solution consisted of a Hewlett-Packard (HP) Model 33120A master function generator that produced a 1 kHz square wave that in turn triggered separate function generators for each laser. A Palkit pulse generator triggered the 2.052-μm pump laser on the falling side of the square wave of the HP while a Stanford Research Systems (SRS) Model DG535 Digital Delay/Function Generator triggered the Nd:YAG laser on the rising side. The SRS was programmed to delay its trigger by 0.19-msec, which, when added to a 0.31-msec lag between triggering the Coherent Infinity laser and the arrival of the 3.6-μm pulse, caused the two pulses to overlap on the next 2.052-μm pulse. The SRS was then instructed to delay 100-msec before looking for the next trigger from the HP. The result was a temporal overlap of the two pulses to within ±50-ns. The exact position of the two pulses could not be determined because the pulses were shorter than the 50-ns time constant of the detector, a liquid-nitrogen-cooled mercury-cadmium-telluride (Hd:Cd:Te) photoconductor. Nevertheless, the time-averaged overlap observed was sufficient for a DFG experiment.

The other major issue in combining the beams was overlapping them spatially. The beams were combined at a flat CaF_2 and directed through a pair of fixed irises. The beams were then adjusted to deliver maximum power to a detector on the far side of the second iris. Next, both beams were focused through a 10-cm focal length CaF_2 lens and the beam waist position of each located with a scanning razor blade. Beam adjustment continued until the half power position (corresponding to the middle of beam) of each beam was identical in both dimensions, to the accuracy of the translating stage (±10-μm).

The pump waist diameter was measured at 50-μm by 150-μm while the signal waist was 170-μm by 300-μm. Both of these beams were much more elliptical than previously noted but no cause could be determined.

The signal beam was polarized in the vertical plane while the pump was polarized horizontally. The pump power was usually limited to 10-mW average power to avoid damaging the crystal faces, but occasional diversions up to 50-mW were attempted. The 3.6-μm signal energy was constant at 3.6-μJ per pulse. The output of the OPGaAs crystal was directed into a 0.15-m Acton Research monochromator whose slits were set wide-open to act as a 200-nm bandpass filter. The monochromator was set to observe 4.780-μm while the signal wavelength was tuned from 3.534- to 3.625-μm.

Results. Once again, no nonlinear photon generation was observed and once again, the lack of phase matching was suspected. In retrospect, however, several experimental flaws could also have led to a negative finding. For example, the signal was tuned over a relatively narrow range (approximately one FWHM). Phase matching may have occurred outside that region. Also, the pump and signal beams were mismatched in beam spot size by a ratio of 3:1. Energy transfer would have been correspondingly lower, possibly below the threshold of the detector. Unfortunately, these deficiencies were not noted until after both samples were damaged beyond usefulness in the final temperature tuning experiment (see below).

OPG Experiment

Background. One other interaction to consider was optical parametric generation (OPG). OPG is simply an OPO without a resonant cavity and can generate significant

amounts of light if the single pass gain is sufficiently large [4]. Furthermore, OPOs require at least one of the generated beams fall within the reflectivity ranges of the OPO mirrors. OPG allows the nonlinear interaction to find the phase-matched frequencies that conserve phase and energy, wherever they may be. However, such an interaction requires tremendous amounts of gain, enough to amplify the signal and idler to detectable levels from noise. Even under the most optimistic conditions, the OPGaAs samples do not generate sufficient gain to be detected with the equipment available to this research.

Procedure. Nevertheless, an attempt was made, out of desperation, to observe OPG with the longer Sample 1. The experimental equipment was identical to that used for the OPO experiment, except that the OPO mirrors where removed. The OPGaAs output was spectrally filtered through a 0.75-m Acton Research monochromator. The entrance and exit slits were again opened to the widest possible setting to maximize throughput, causing the monochromator to act as a scanable 200-nm bandpass filter. A Au:Ge detector cooled to 77°K was placed at the exit slit to observe wavelengths from 1.8- to 4.3-μm. The pump beam polarization angle was set to 45° from the vertical, near the maximum d_{eff} as determined in Appendix A.

Results. As expected, no detectable nonlinear emission was noted. By the one-photon per mode noise model presented by Byer and others, the lack of results is no surprise [10]. The energy of one 3.6-μm photon amplified even 100 times in one pass would not have reached the detection threshold of the liquid nitrogen-cooled Au:Ge detector.

DFG Experiment with Temperature Tuning

Background. This experiment was never completed because the AR coatings on Sample 2 began flaking off after two heating-cooling cycles. However, the theory behind the experiment is still valid, so the procedures and the theory will be reviewed here. It is well known that the index of refraction of most materials changes with temperature. As it changes, the signal and idler wavelengths that satisfy the phase matching relationship change as well. This characteristic has long been used to tune the output of OPOs by adjusting the temperature of the non-linear crystal with a crystal oven and is well modeled in many non-linear optical materials. A team from Stanford University produced such a model to predict the temperature-induced changes in the refractive index of GaAs [28]. Their model assumed that index changes could be modeled (according to perturbation theory) as a Taylor series expansion about the room temperature index value predicted by Pikhtin4. The team monitored the evolution of the interference fringes created by a bulk sample of plane-parallel polished GaAs in a Fourier Transform infrared interferometer. By observable in the resulting interferogram, they measured both the rate of change of refractive index versus temperature and the first derivative of that rate. These empirical value were then applied to the following Taylor series expansion:

$$n(T) = n(T_o) + \frac{\partial n}{\partial T}(T - T_o) + \frac{\partial^2 n}{\partial T^2}(T - T_o)^2 \qquad \textbf{(21)}$$

where T is the temperature of interest, T_o is the reference room temperature (23°C) and the higher order terms of the series have been ignored. Application of this temperature tuning correction to Pikhtin4 and the phase matching condition (Equation 15) resulted in a prediction of quasi-phase matching for a periodicity of 58.8-μm at an OPGaAs

temperature of 103°C. It should be noted that the Stanford temperature correction was based on data collected between 25°C and 90°C, so an extrapolation to 103°C may not be valid. Furthermore, the data upon which Pikhtin4 is based was not collected at room temperature and thus may not be valid at room temperature as assumed by the Stanford University team. Nevertheless, a second DFG experiment was devised to test this new information.

Procedure. The same equipment from the first DFG experiment was used in this attempt. A copper Omega-controlled crystal oven was added to the crystal mount to change the sample temperature. The controller featured a thermocouple sensor for closed loop-control of the temperature. No calibration of this thermocouple was made and no limit was set on the time-rate-of-change of the temperature controller, which heated at a rate of approximately 1°C every 4 seconds. OPGaAs Sample 2 was heated to 100°C and pumped with a 1-kHz-pulsed 5-mW beam with a 100-μm beam diameter. However, the alignment of the pump beam took place at the end of the day. When the crystal was reheated the next day in preparation for signal beam alignment, discoloration was noted on the end surfaces. A closer examination revealed that the AR coatings had begun to peel and flake off (see Figure 12 a). Unfortunately, OPGaAs Sample 2 had been broken the previous day when it was removed from its mount and rendered unusable.

Results. No conclusions can be drawn from this experiment because it was not completed due to the loss of the samples. One not-so-new finding was the fact that the materials used in AR coatings often have different thermal expansion rates than the sub-surfaces on which they are deposited. If an AR-coated crystal is heated too quickly, the rapid thermal expansion can severely stress the coatings to the point that they can

separate. Therefore, any AR-coated material must be heated and cooled slowly. Indeed, Gonzalez recommended changing the temperature at no more than 5°C per minute and leaving the crystal oven on continuously to minimize stress to the coatings [21:98]. With both samples destroyed, the experimental efforts came to a close.

IV. Summary and Recommendations

Summary

In an effort to understand why the experiments of the research effort did not achieve quasi-phase matching with any technique while other researchers did, the results of Levi, et al's DFG experiment were reverse engineered and compared to the phase matching parameters predicted by Piktin3, Pikhtin4, and Tanguy [31, 39, 49]. Levi, et al, provided an example of quasi-phase matching occurring for a pump wavelength of 1306.7-nm and a signal wavelength of 1567-nm. The OPGaAs crystal was 19 mm long with a 13.15-μm coherence length. In the figure presenting the phase matching curve for this combination, Levi, et al, stated that the position of the predicted peak was shifted slightly to line up with the measured data. The researchers cited Pikhtin and Yas'kov as their Sellmeier equation source, but they did not specify which equation was used. Therefore, the phase matching condition (Equation 2) was solved for both Pikhtin refractive index formulations. Tanguy's solution was also included for comparison. The results are presented in Table 2.

Using the Pikhtin3 formulation, a coherence length of 12.50-μm was predicted, far from the 13.15-μm length specified in the paper. Pikhtin4 was closer, predicting phase matching at 1572.1-nm. This would have required only a 5.1-nm shift on Levi et al's figure and thus is probably the equation they used to design the samples (a fact later confirmed by e-mail) [17]. Tanguy's equation, however, predicted a phase-matched interaction for a signal at 1565.8-nm, much closer to Levi's data than either of the Pikhtin equations. One might speculate that the actual solution for the refractive index of GaAs

Table 2. Phase matching solutions for Levi's experiment.

	Reported	Pikhtin3	Pikhtin4	Tanguy
Coherence length (μm)	13.15	12.50	13.30	13.11
Peak wavelength (nm)	1.567	1.5505	1.5721	1.5658
Difference from reported peak wavelength (nm)	---	-16.5	+5.1	+1.2

in the mid-IR lies somewhere between Pikhtin4 and Tanguy. It must be noted, however, that a similar analysis for SHG with a 10.5-μm pump in quasi-phase matched GaAs has the Tanguy formulation over-predicting the required period by a factor of five while both Pikhtin equations produce more reasonable values. Clearly, no one equation is correct for the entire 3-15-μm region and further research in this area is warranted.

Recommendations

Materials. Quasi-phase matching is highly dependent on accurate formulations for the index of refraction of the material of interest. Those available in the literature for GaAs are not accurate enough in the mid-IR. As demonstrated in Chapter II, variations as small as 0.01% among formulations produce vastly different coherence length solutions. The refractive index of GaAs should be precisely measured in the 2-μm to 5-μm region and the subsequent fit of the Sellmeier equation to the data will require an accuracy to at least four decimal places. Tanguy remarked that any such high precision measurements of refractive index must account for the relative refractive index of air, which is not exactly equal to one [49:1750]. Furthermore, at the required level of

accuracy, the effects of residual GaAs doping from impurities cannot be ignored in the transparency region [33:1241, Sell]. Therefore, the residual doping of the OPGaAs by its germanium substrate or other trace materials may have to be considered.

The optical quality of the OPGaAs samples must be improved as well. Neither of the samples allowed a large-diameter beam to pass through aberration-free. Only Sample 2 provided reasonable optical clarity for very small beams. However, such small beams are difficult to align and become inefficient beyond the tight focusing limit. In addition, the end faces of the crystals should be parallel-plane polished eliminate crystal wedge and simplify the OPO cavity alignment process. Since GaAs is not transparent to visible light, the cavity alignment is possible only by bouncing an alignment beam from a visible laser off of the crystal faces. Any significant wedge in the crystal makes this process much more difficult.

If the same Tm:Ho:YLF pump laser is retained for future research, then a variety of GaAs samples with varying periodicities are required. Assuming the same OPO optics will also be retained, a study of the OPO cavity bandwidth was performed using the Pikhtin4 and Tanguy index formulations (see Figure 14). The most promising domain lengths for quasi-phase matching appear to be 30.0-, 30.5- 31.0- and 31.5-μm (see Figure 15). These lengths were selected to increase the chances that one or more samples would be quasi-phase matched by either formulation.

In addition to more samples, the manufacturing of longer samples would also be desirable. Longer samples would increase the available gain per pass, causing the OPO to reach threshold more quickly. Since the OPO single pass signal gain is proportional to

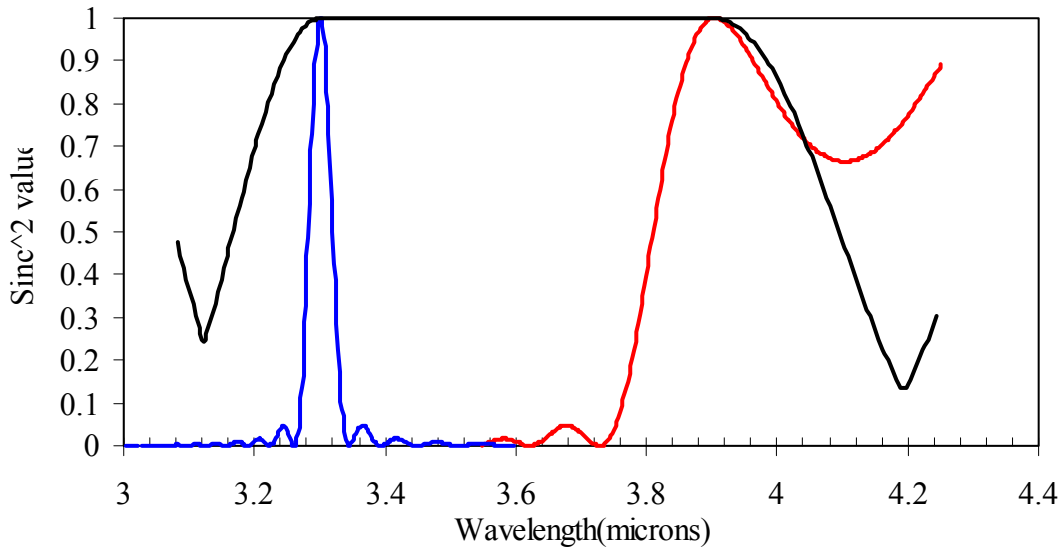

Figure 14. Spectral range of OPO optics. The wide black curve represents the range over which the dichroic OPO mirrors are highly reflective. The red and blue curves are the quasi-phase matched curves of signal beams at 3.9- and 3.3-µm, respectively.

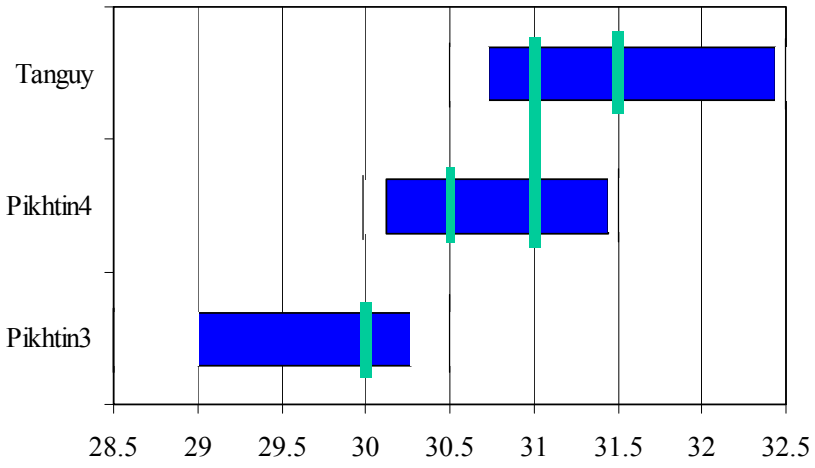

Figure 15. Quasi-phase matching ranges for Pikhtin3, Pikhtin4, and Tanguy index formulations. The blue horizontal bars represent the ranges of coherence lengths that are quasi-phase matched to a 2.052-µm pump laser and that will resonate with the reflectivity range of the OPO optics. The green vertical bars indicate the recommended coherence lengths for future experimentation.

the square of the length in isotropic materials, a doubling of the sample length could lead to a four-fold increase in gain (at threshold) and a corresponding decrease in OPO threshold.

Procedures. Besides improvements in the OPGaAs material, two general areas for improvement in experimental procedures were noted. The first involves additional testing with the a new pump laser and the existing samples. The second, much broader category involves experimental techniques and procedures that apply to any nonlinear optical experiment.

If additional experiments are planned with the current samples, three major points must be considered. First, the samples are no longer optically flat on their endfaces and need to be plane-parallel polished to a laser quality finish. Sample 1 may be completely unusable, however, due to stress fractures in the crystal created when the sample was dropped on the floor. The crystal should first be examined internally in the IR under high magnification to determine the severity of the stress cracking. Second, a pump laser of another wavelength is required. If Tanguy's Sellmeier formulation is correct, then the pump laser must have a wavelength of no more than 2.023-μm to achieve quasi-phase matching. A tunable laser in this range would the ideal way to explore the phase matching envelope of the current OPGaAs samples. The final consideration is Brewster angle pumping. The raw faces of the OPGaAs might tempt one to use Brewster's angle to minimize reflective losses of the pump beam. However, the beam can only transit the crystal at Brewster's angle if polarized along the horizontal ([0 1 1])direction because the crystals are very thin compared to their lengths. The polarization study accomplished in Appendix A show the signal and idler to prefer a 54.7° angle for such a pump beam

orientation. Obviously, these resonated beams would not completely satisfy the Brewster's angle criteria when transiting the crystal face and would experience greater loss at the interfaces than the pump.

Regardless of what equipment or samples are used, several procedural changes in the experiments reported here would benefit any future research. For example, any future OPGaAs samples should be examined for transparency before being AR-coated. If sufficiently transparent areas are noted, then DFG experiments should be attempted with widely tunable signal and pump lasers to detect signs of nonlinear interactions. Once (or if) DFG is demonstrated, only then should a researcher go thorough the trouble of coating the samples and attempt an OPO, armed with knowledge of the exact phase matching parameters. In another procedural point, any AR coatings on the OPGaAs samples must be able to withstand 1.5-2-J/cm^2 at pulses ranging from 40-100-ns. A special effort should be made to verify this performance level with the vendor before purchase so that coating damage is no longer a limiting issue. Next, the shortest possible OPO cavities should be used to decrease rise time required to reach threshold. In fact, shorter cavities would allow the use of shorter pulse lengths and higher peak power. However, the tradeoff between peak power and damage threshold must be considered. Finally, if temperature tuning is used to adjust the OPO output of a coated OPGaAs sample, one must control the thermal gradient to minimize the chance of overstressing any AR coatings due to different thermal expansion rates.

Together, the recommendations for materials and procedural techniques constitute the major (and only!) contribution of this research to the body scientific. Although most of the lessons learned from these experiments are not new, they will serve, at the least, as

a record of what did not work and as a guide to more successful attempts in the future. GaAs, with its wide transparency range and strong nonlinear coefficient, offers significant theoretical promise to the IR countermeasures and remote sensing fields. It only awaits a demonstrable OPO to become practical.

Appendix A: D_{eff} in GaAs

GaAs is an isotropic material in the $\bar{4}3\,\mathrm{m}$ crystal class [54:511]. For this type of crystal, the polarization equation (Equation 5) takes the following form:

$$\begin{bmatrix} P_{NL-x}(\omega_3) \\ P_{NL-y}(\omega_3) \\ P_{NL-z}(\omega_3) \end{bmatrix} = 2\varepsilon_o \begin{bmatrix} 0 & 0 & 0 & d_{14} & 0 & 0 \\ 0 & 0 & 0 & 0 & d_{25} & 0 \\ 0 & 0 & 0 & 0 & 0 & d_{36} \end{bmatrix} \begin{bmatrix} E_x(\omega_1)E_x(\omega_2) \\ E_y(\omega_1)E_y(\omega_2) \\ E_z(\omega_1)E_z(\omega_2) \\ E_y(\omega_1)E_z(\omega_2)+E_z(\omega_1)E_y(\omega_2) \\ E_x(\omega_1)E_z(\omega_2)+E_z(\omega_1)E_x(\omega_2) \\ E_x(\omega_1)E_y(\omega_2)+E_y(\omega_1)E_x(\omega_2) \end{bmatrix}. \quad \textbf{(22)}$$

where $d_{14} = d_{25} = d_{36}$. In this experiment, the pump beam propagated along the [0 1 1] direction. Therefore, its polarization vector was normal to this direction, in the (0 1 1) plane (see Figure 16). The x-, y-, and z-components of the electric fields were defined as

$$\begin{aligned} E_x(\omega) &= \cos(\theta)|E| \\ E_y(\omega) &= \sin(\theta)\cos(\phi)|E| \\ E_z(\omega) &= \sin(\theta)\sin(90^\circ+\phi)|E| \end{aligned} \quad \textbf{(23)}$$

with the θ and ϕ angles defined as indicated in Figure 16. These angles do not follow the standard for spherical coordinates for ease of calculation [43]. For the [0 1 1] propagation direction, ϕ=45° and the sine terms operating on ϕ reduce to $\pm\sqrt{2}/2$. Substituting Equation 21 into Equation 20 results in

$$\begin{aligned} P_{NL-x}(\omega_i) &= -2\varepsilon_o d_{14}(\sin(\theta_p)\sin(\theta_s))\cdot|E_p|\cdot|E_s|. \\ P_{NL-y}(\omega_i) &= 2\varepsilon_o d_{14}\left(\frac{\sqrt{2}}{2}\sin(\theta_p)\cos(\theta_s)+\frac{\sqrt{2}}{2}\cos(\theta_p)\sin(\theta_s)\right)\cdot|E_p|\cdot|E_s| \\ P_{NL-z}(\omega_i) &= -2\varepsilon_o d_{14}\left(\frac{\sqrt{2}}{2}\sin(\theta_p)\cos(\theta_s)-\frac{\sqrt{2}}{2}\cos(\theta_p)\sin(\theta_s)\right)\cdot|E_p|\cdot|E_s| \end{aligned} \quad \textbf{(24)}$$

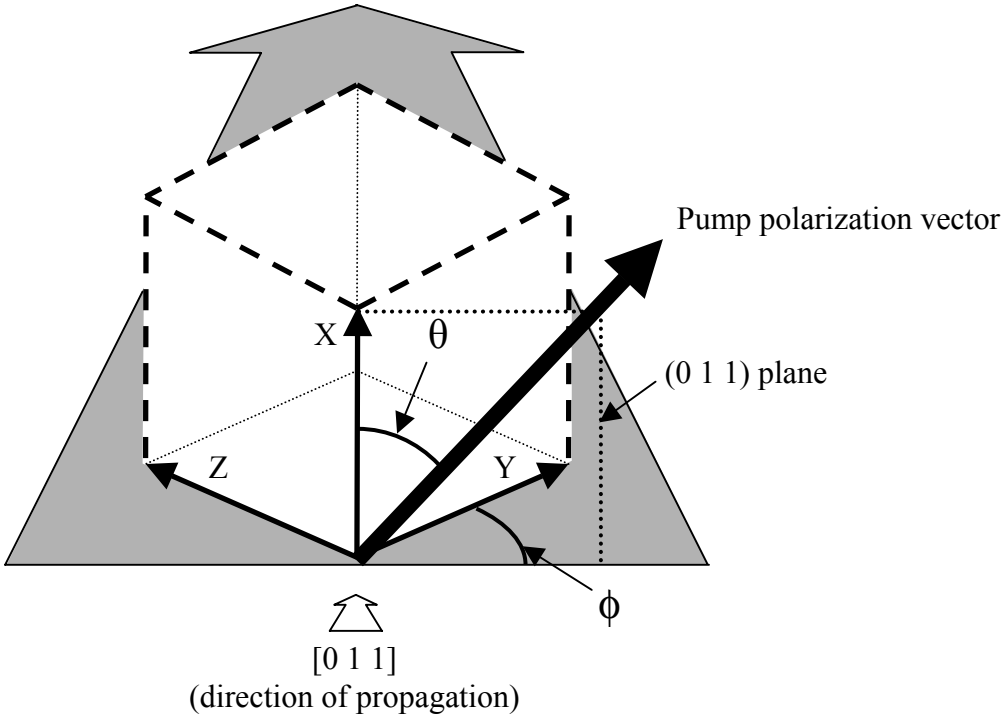

Figure 16. OPGaAs crystal orientation. The angle θ is defined from the x-axis in the (0 1 1) plane and ϕ is defined from the y-axis in the (1 0 0) plane. This nonstandard spherical coordinate system was used for ease of calculation since the three beams are polarized in the (0 1 1) plane.

Equation 22 assumes a pump wave will interact with a signal wave to produce an idler wave with the polarization vector as indicated. It should be noted that the polarization vector of the idler is perpendicular to the direction of propagation ([0 1 1]) for any combination of pump and signal polarization vector directions, a fact that can be confirmed by performing a dot-product between the vector and the direction. The d_{14} term was chosen here to represent the individual nonlinear coefficients (since they are all equal in GaAs). The effective nonlinear coefficient, d_{eff}, can now be found from the magnitude of the three components of Equation 22 as follows:

$$\left|\vec{P}_{NL}(\omega_i)\right| = \frac{2}{m\pi} d_{14} \sqrt{P_{NL-x}(\omega_i)^2 + P_{NL-y}(\omega_i)^2 + P_{NL-z}(\omega_i)^2} \qquad \textbf{(25)}$$

$$\left|\vec{P}_{NL}(\omega_i)\right| = 2\varepsilon_o \frac{2}{m\pi} d_{14} \sqrt{\left(\sin(\theta_p)\sin(\theta_s)\right)^2 + 2\left(\frac{\sqrt{2}}{2}\right)^2 \left(\sin(\theta_p)\cos(\theta_s) + \cos(\theta_p)\sin(\theta_s)\right)^2} \left|E_p\right| \cdot \left|E_s\right| \quad \textbf{(26)}$$

$$\left|\vec{P}_{NL}(\omega_i)\right| = 2\varepsilon_o d_{eff} \cdot \left|E_p\right| \cdot \left|E_s\right| \quad \textbf{(27)}$$

where $$d_{eff} = \frac{2}{m\pi} d_{14} \sqrt{\left(\sin(\theta_p + \theta_s)\right)^2 + \left(\sin(\theta_p)\sin(\theta_s)\right)^2} \quad \textbf{(28)}$$

The $\frac{2}{m\pi}$ term comes from the duty cycle of the periodically-modulated nonlinear coefficient in quasi-phase matched materials [35:2103]. For the 50% duty cycle in the experimental OPGaAs samples, m = 1. Equation 24 clearly indicates that the effective nonlinear coefficient will vary drastically depending on the specified polarization angles.

Several authors have examined the optimal polarization angles for DFG experiments in GaAs [29,48:2030,55:1011]. In a DFG design, one must specify the polarization angle of both the pump and the idler beams. Each of the authors reported a maximum d_{eff} when both beams were polarized along the [1 1 1] family of directions. However, for an OPO, only the pump beam polarization angle is specified. Because GaAs is isotropic, the other two beams may be polarized along any angle, but only the combination of signal and idler waves with the greatest gain will be amplified. A methodical investigation of Equation 24 was made by evaluating the expression for every possible combination of θ_p and θ_s from -π to π. For each value of θ_p, θ_s varied over the range and the maximum d_{eff} was noted as $\frac{4}{\sqrt{3}\pi} d_{14} = 0.74\ d_{14}$. The results are displayed in Figure 17, along with Zheng, et al's results for parallel- and orthogonally-polarized

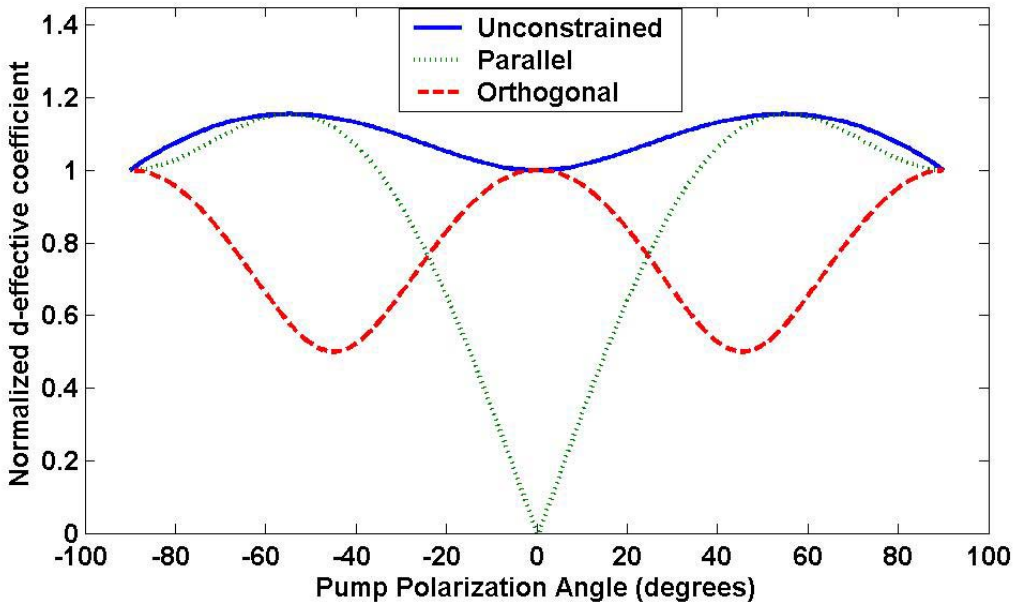

Figure 17. Theoretical effective nonlinear coefficient deff as a function of the angle between the pump beam polarization vector and the OPGaAs [0 0 1] direction. The two dashed curves duplicate Zheng's findings for signal beams polarized parallel and orthogonal to the pump [55:1011]. The solid line results when the angle between the pump and signal polarization is unconstrained.

pump and signal beams. The maximum d_{eff} was found at $\theta = 54.7°$, which corresponds to the $[1\ 1\ \bar{1}]$ direction, which is equivalent to the [1 1 1] direction and in agreement with the previous findings. Notably for the OPO case, however, d_{eff} remains within 15% of the maximum for the entire range of angles. Furthermore, the signal and idler polarization angles are always parallel (except at $\theta = 0°$ and 90°, where they can be either parallel or orthogonal) and were not necessarily orthogonal to the pump beam. Figure 18 illustrates this point.

This analysis reveals several theories about the design and operation of OPGaAs OPOs that have not previously been noted in the published literature. First, there is no "bad" polarization angle at which to pump the crystal. Any angle will access a

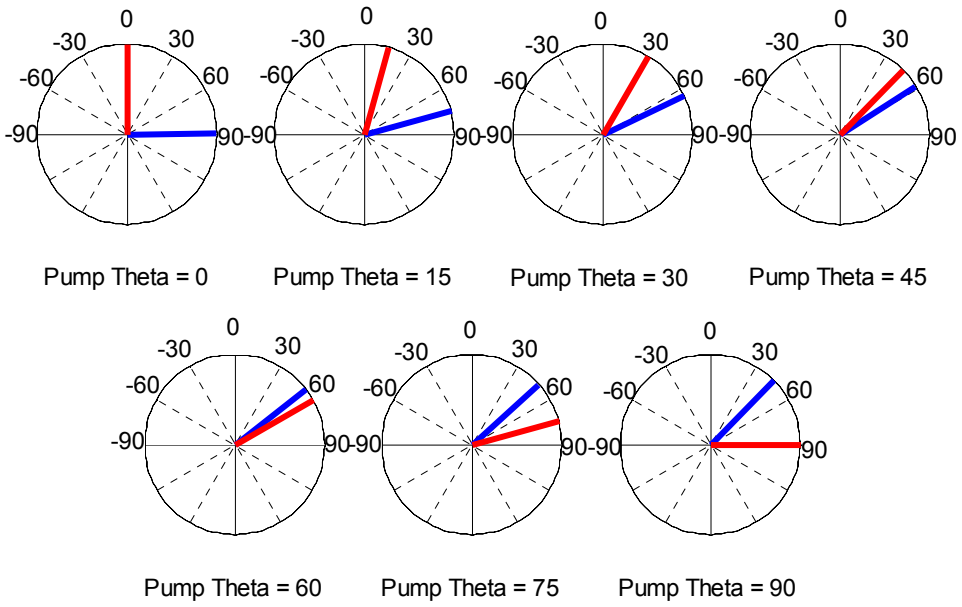

Figure 18. Effect of pump polarization angle on signal and idler polarization angle. The blue lines show the signal and idler polarization angles that result in the maximum d_{eff} for the indicated pump beam polarizations, displayed in red.

significant nonlinear coefficient. Second, the current 0.5-mm-thick crystal samples are not suitable for operations at Brewster's angle. Although such an interface would in nearly perfect transmission and eliminate the need for an AR coating, the OPGaAs crystal are too thin to allow the beams to propagate the entire length without encountering one of the side faces. Finally, the signal and idler polarization angles could be rotated if desired by simply changing the pump polarization angle during laser operation. This capability to arbitrarily select OPO output polarization is not available in most other traditional quasi-phase matched materials.

Appendix B: OPO Cavity Design

One of the central features of an optical parametric oscillator (OPO) is the resonant cavity that contains the oscillating parametric field. Because the OPO contains a nonlinear crystal, the design of such a cavity is not trivial. This appendix describes the process for designing a symmetrical resonant cavity containing a block of optically-dense material.

The OPO cavity design used for this research is presented in Figure 19. The cavity mirrors were a pair of CaF_2 meniscus lenses anti-reflection-coated to pass the pump and idler beams and high-reflection-coated to resonate the signal beam. The mirrors were available in pairs with radii-of-curvature of 5- and 10-cm and were mounted in adjustable lens holders. The OPGaAs sample was placed on a movable stage equidistant between the mirrors. The distance between each mirror and its corresponding crystal face was adjusted by hand to an accuracy of approximately ±1-mm. As will be seen below, this level of positioning accuracy is insufficient for extremely small beam sizes. Future designers should consider mounting the lens holders on micro-adjustable stages that can be translated along the direction of propagation, if precision positioning of the lenses is required.

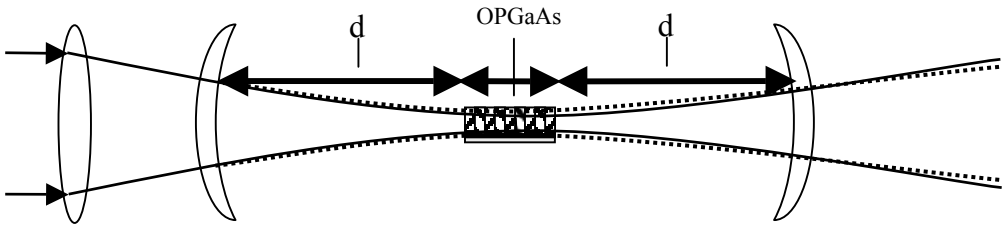

Figure 19. OPO cavity.

The cavity was designed using the ABCD method. The cavity unit cell is pictured in Figure 20 along with the ABCD matrix for each section. With the crystal face designated as the cavity starting point, the transmission matrix of the unit cell is

$$M = \begin{bmatrix} 1 & \frac{L}{n} \\ 0 & 1 \end{bmatrix} \begin{bmatrix} 1 & d \\ 0 & 1 \end{bmatrix} \begin{bmatrix} 1 & 0 \\ \frac{-2}{R} & 1 \end{bmatrix} \begin{bmatrix} 1 & d \\ 0 & 1 \end{bmatrix} \tag{29}$$

where L is the length of the OPGaAs sample, n is the refractive index for the wavelength of interest, d is the distance between the OPO mirror and the crystal face and R is the radius of curvature of the pair of lenses. The crystal face is used as the starting point because the beam waist cannot be measured inside the crystal. The transmission matrix simplifies to a 2x2 matrix:

$$M = \begin{bmatrix} A & B \\ C & D \end{bmatrix} = \begin{bmatrix} \frac{-2L + Rn - 2dn}{Rn} & \frac{LR - 2Ld + 2dnR - 2d^2 n}{Rn} \\ \frac{-2}{R} & \frac{R - 2d}{R} \end{bmatrix} \tag{30}$$

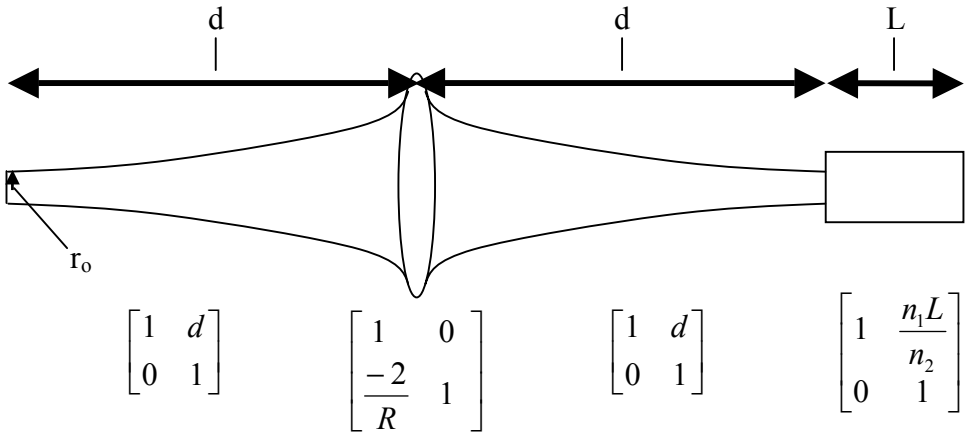

Figure 20. OPO unit cell. R is the radius of curvature of the meniscus lenses. This design assumes both lenses have the same curvature. n_1 and n_2 are the refractive indices of air and GaAs, respectively. The ABCD matrices appear below their relevant section of the system.

Using the relation

$$w_c = \sqrt{\frac{\lambda_0}{\pi n}\frac{B}{\sqrt{1-\left(\frac{A+D}{2}\right)^2}}} \tag{31}$$

we obtain the beam radius at the crystal face as:

$$w_c = \sqrt{\frac{\lambda_0}{\pi n}\frac{\frac{LR-2Ld+2dnR-2d^2n}{Rn}}{\sqrt{1-\left(1-\frac{2d}{R}-\frac{L}{Rn}\right)^2}}} \tag{32}$$

Using Equation 32, the distances required for a variety of beam waists are presented in Table 3. A plot of Equation 32 is presented in Figure 21. One notes that for beam waists smaller than 60-μm, the precision with which the lenses must be positioned increases dramatically.

Table 3. OPO cavity design parameters.

L = 1.4-cm				
R = 10-cm			R = 5-cm	
w_o (μm)	d (cm)		w_o (μm)	d (cm)
130	5.92		93	2.61
125	6.97		90	3.22
100	8.88		80	4.00
75	9.53		75	4.21
60	9.69		60	4.58
50	9.75		50	4.70
40	9.78		40	4.77

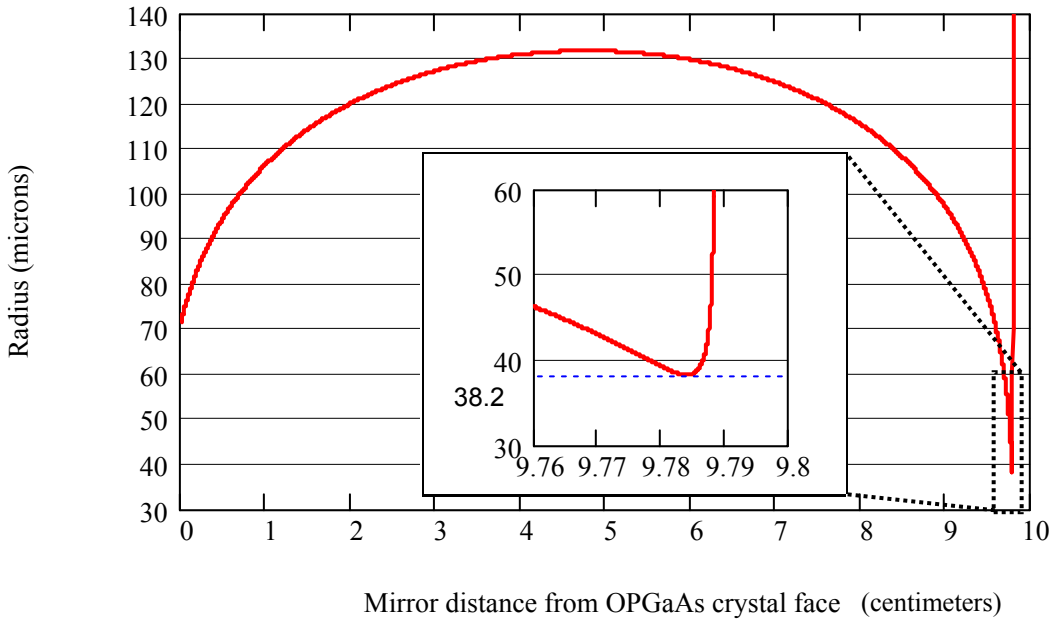

Figure 21. Radius of the resonant gaussian mode at OPGaAs crystal face. L = 1.4-cm, R = 10-cm, n(λ_o = 3.6-μm) = 3.3082 . The inset graph shows the minimum beam radius at the crystal face.

Appendix C: OPO Threshold Calculations

Constants

$\varepsilon o := \left(8.854187817 \cdot 10^{-12}\right) \frac{C^2}{N\,m^2}$ $\quad c := 299792458 \frac{m}{s}$

Wavelengths

$\lambda p := 2.052 \mu m$

$\lambda s := 3.6 \mu m$

$\lambda i := \frac{1}{\left(\frac{1}{\lambda p} - \frac{1}{\lambda s}\right)}$

$\lambda i = 4.772\,\mu m$

Radial Frequency

$\omega p := \frac{2 \cdot \pi \cdot c}{\lambda p}$ $\omega p = 9.18 \times 10^{14} \frac{1}{s}$

$\omega s := \frac{2 \cdot \pi \cdot c}{\lambda s}$ $\omega s = 5.232 \times 10^{14} \frac{1}{s}$

$\omega i := \frac{2 \cdot \pi \cdot c}{\lambda i}$ $\omega i = 3.947 \times 10^{14} \frac{1}{s}$

Refractive Index (ref: Tangu

$npum := 3.3383$

$nsig := 3.3082$

$nidl := 3.3021$

OPGaAs Nonlinear Coefficient

$pm := 10^{-12} m$ $\quad d14 := 86 \cdot \frac{pm}{V}$ $\quad deff := \frac{4}{\pi \cdot \sqrt{3}} \cdot d14$ $\quad deff = 63.219 \frac{pm}{V}$

OPGaAs OPO

OPO Cavity Length: $Lcav := 20cm$

OPGaAs Sample 2 length: $L := 1cm$

OPGaAs actual length: $Lcry := 1.4cm$

Spot size radius $r := 100 \cdot \mu m$

Pump pulse rate $f := 1000Hz$

Pump pulse duration (FWHM) $\tau p := 100ns$

Approximated loss term

$Rmirrors := 0.99$ absorption $\alpha := 0.075 \cdot \frac{1}{cm}$

$Rrt := Rmirrors^2 \cdot e^{-2 \cdot \alpha \cdot Lcry}$

$art := 1 - Rrt$

$art = 0.206$

Correct loss term

$\alpha sp := -\ln(Rmirrors) + \alpha \cdot Lcry$

$2 \cdot \alpha sp = 0.23$

Poor mode matching

$wp := r \quad ws := 1.5 \cdot r$

$gmm := \frac{2 \cdot wp^2}{wp^2 + ws^2}$ $\quad gmm = 0.615$

SRO threshold increase for square pump pulse of durationtp

$Nx := \left(1 + \frac{Lcav \cdot \ln\left(10^{12}\right)}{2 \cdot \tau p \cdot c \cdot \alpha sp}\right)$ $\quad Nx = 1.801$

Pump Threshold - CW

$$Ith\_cw\_ := \frac{npum \cdot nsig \cdot nidł \cdot \varepsilon o \cdot c^3}{\omega i \cdot \omega s \cdot L^2 \cdot deff^2} \cdot \frac{art}{1 - art}$$

$$Ith\_cw\_ = 2.727 \times 10^6 \frac{W}{cm^2}$$

Pump Threshold - with losses

$$Ith\_lossy := \frac{npum \cdot nsig \cdot nidł \cdot \varepsilon o \cdot c^3}{\omega i \cdot \omega s \cdot L^2 \cdot deff^2} \cdot \frac{2 \cdot \alpha sp}{1 - 2 \cdot \alpha sp} \cdot Nx \cdot \frac{1}{gmm}$$

$$Ith\_lossy = 1.537 \times 10^7 \frac{W}{cm^2}$$

$$\frac{Ith\_lossy}{Ith\_cw\_} = 5.637$$

For τp = 100-ns and r = 100-μm,

$$Ith\_cw\_ = 2.727 \times 10^6 \frac{W}{cm^2}$$

$$Ith\_lossy = 9.22 \times 10^6 \frac{W}{cm^2}$$

$$\frac{Ith\_lossy}{Ith\_cw\_} = 3.381$$

Bibliography

1. Barcus, L. C., A. Perlmutter, and J. Callaway. "Effective mass of electrons in gallium arsenide," *Physical Review*, 111, 167-168 (1 July 1958).

2. Barnes, Norman P., Keith E. Murray, Mahendra G. Jani, and Sarah R. Harrell. "Diode-pumped Ho:Tm:YLF laser pumping an $AgGaSe_2$ parametric oscillator," *Journal of the Optical Society of America – B*, 11, 2422-2426 (December 1994).

3. Blakemore, J. S. "Semiconducting and other major properties of gallium arsenide." *Journal of Applied Physics*, 53, R123-R181 (October 1982).

4. Boyd, G. D. and D. A. Kleinman. "Parametric interaction of focused Gaussian light beams," *Journal of Applied Physics*, 39, 3597-3639 (July 1968) in *Selected Papers on Optical Parametric Oscillators and Amplifiers and Their Applications*, Vol. MS 140, Jeffrey H. Hunt, editor. Bellingham, WA: SPIE Optical Engineering Press, 1997.

5. Boyd, Robert W. *Nonlinear Optics*, New York: Academic Press, 1992.

6. Bravetti, P., A. Fiore, V. Berger, E. Rosencher, J. Nagle, and O. Gauthier-Lafaye. "5.2-5.6-μm source tunable by frequency conversion in a GaAs-based waveguide," *Optics Letters*, 23, 331-333 (1 March 1998).

7. Broderick, N. G. R., G. W. Ross, H. L. Offerhaus, D. J. Richardson and D. C. Hanna. "Hexogonally poled lithium niobate: a two dimensional nonlinear photonic crystal," *Physical Review Letters*, 84,4345-4348 (2000).

8. Budni, P. A., L. A. Pomeranz, M. L. Lemons, C. A. Miller, J. R. Mosto, and E. P. Chiklis. "Efficient mid-infrared laser using 1.9-μm-pumped Ho:Yag and $ZnGeP_2$ optical parametric oscillators," *Journal of the Optical Society of America – B*, 17, 723-728 (May 2000).

9. -----, P. A., M. G. Knights, E. P. Chicklis, and K. L. Schepler. "Kilohertz $AgGaSe_2$ optical parametric oscillator pumped at 2 μm," *Optics Letters*, 18, 1068-1070 (1 july 1993).

10. Byer, Robert L. "Optical Parametric Oscillators," in *Quantum Electronics, Volume I – Non-linear Optics, Part B*, Eds Herbert Rabin and C.L. Tang. New York: Academic Press, 1975.

11. -----, Robert L. "Quasi-phasematched nonlinear interactions and devices," *Journal of Nonlinear Optical Physics & Materials*, 6, 549-592 (December 1997).

12. Choy, Michael M. and Robert L. Byer. "Accurate second-order susceptibility measurements of visible and infrared nonlinear crystals," *Physical Review – B*, 14, 1693-1706 (15 August 1976) in *Selected Papers on Optical Parametric Oscillators and Amplifiers and Their Applications*, Vol. MS 140, Jeffrey H. Hunt, editor. Bellingham, WA: SPIE Optical Engineering Press, 1997.

13. Ebert, Christopher B., Loren A. Eyres, Martin M. Fejer, and James S. Harris, Jr. "MBE growth of antiphase GaAs films using GaAs/Ge/GaAs heteroepitaxy." *Journal of Crystal Growth*, 201-202: 187-193 (1999).

14. Eckardt, R. C., Y. X. Fan, R. L. Byer, C. L. Marquardt, M. E. Storm, and L. Esterowitz. "Broadly tunable infrared paramteric oscillator using $AgGaSe_2$, *Applied Physics Letters*, 49, 608-610 (15 September 1986) in *Selected Papers on Optical Parametric Oscillators and Amplifiers and Their Applications*, Vol. MS 140, Jeffrey H. Hunt, editor. Bellingham, WA: SPIE Optical Engineering Press, 1997.

15. Eyres, L. A., P. J. Tourreau, T. J. Pinguet, C. B. Ebert, J. S. Harris, Jr, M. M. Fejer, B. G. Gerard, L. Becouarn, and E. Lallier. "All-epitaxial orientation-patterned GaAs for nonlinear optical frequency conversion." *2000 IEEE Leos Annual Meeting Conference Proceedings*. IEEE: 2000.

16. Fejer, Martin M., G. A. Magel, Deiter H. Jundt, and Robert L. Byer. "Quasi-phase-matched second harmonic generation: tuning and tolerances," *IEEE Journal of Quantum Electronics*, 28, 2631-2654 (November 1992).

17. -----, Martin M. Electronic communication (16 January 2002).

18. Feldman, Albert, and Roy M. Waxler. "Dispersion of the piezobirefrengence of GaAs due to strain-dependent lattice effects," *Journal of Applied Physics*, 53, 1477-1483 (March 1982).

19. Feynman, Richard P. and others. *The Feynman Lectures on Physics – Mainly Mechanics, Radiation, and Heat*. Reading, PA: Addison-Wesley Publishing Company, 1966.

20. Giordmaine, J. A. and Robert C. Miller. "Tunable coherent parametric oscillation in $LiNbO_3$ at optical frequencies," *Physical Review Letters*, 14, 973-976 (14 June 1965) in *Selected Papers on Optical Parametric Oscillators and Amplifiers and Their Applications*, Vol. MS 140, Jeffrey H. Hunt, editor. Bellingham, WA: SPIE Optical Engineering Press, 1997.

21. Gonzalez, Leonel P. *Continuous Wave Singly Resonant Intracavity Optical Parametric Oscilators Using Periodically Poled $LiNbO_3$.* MS thesis. University of Dayton, Ohio, December 1997.

22. Gordon, L., G. L. Woods, R. C. Eckardt, R. R. Route, R. S. Feigelson, M. M. Fejer, and R. L. Byer. "Diffusion-bonded stacked GaAs for quasi-phasematched second-harmonic generation of a carbon dioxide laser," *Electronics Letters*, 29, 1942-1944 (28 October 1993).

23. Harris, Stephen E. "Tunable optical parametric oscillators," *Proceedings of the IEEE*, 57, 2096-2113, (December 1969) in *Selected Papers on Optical Parametric Oscillators and Amplifiers and Their Applications*, Vol. MS 140, Jeffrey H. Hunt, editor. Bellingham, WA: SPIE Optical Engineering Press, 1997.

24. Jannery, Beth. "Directed energy warfare – Something for a Star Wars sequel?" *Journal of Electronic Defense*, n. pag. http://www.jlab.org/news/internet/1997 /warfare.html 24 May 2001.

25. Koh, Shinji, Takashi Knodo, Yasuhiro Shiraki, and Ryoichi Ito. "GaAs/Ge/GaAs sublattice reversal epitaxy and its application to nonlinear optical devices." *Journal of Crystal Growth*, 227-228: 183-192 (2001).

26. Komine, H., W. H. Long, Jr, J. W. Tully, and E. A. Stappaerts. "Quasi-phase-matched second harmonic generation by use of a total-internal-reflection phase shift in gallium arsenide and zinc selenide plates," *Optics Letters*, 23, 661-663 (1 May 1998).

27. Kovalchuk, E. V., D. Dekorsy, A. I. Lvovsky. "High-resolution doppler-free molecular spectroscopy with a continuous-wave optical parametric oscillator," *Optics Letters*, 26, 1430-1432 (15 Sep 2001).

28. Kuo, Paulina S. Electronic communication, 29 November 2001.

29. Lallier, E., L. Becouarn, M. Brevignon, and J. Lehoux. "Infrared difference frequency generation with quasi-phase-matched GaAs," *Electronics Letters*, 34, 1609-1611 (6 Aug 1998).

30. -----, E., M. Brevignon, and J Lehoux. "Efficient second harmonic generation of a CO_2 laser with a quasi-phase-matched GaAs crystal," *Optics Letters*, 23, 1511-1513 (1 October 1998).

31. Levi, O., T. J. Pinguet, T. Skauli, L. A. Eyres, L. Scaccabarozzi, M. M. Fejer, J. S. Harris, Jr, T. J. Kulp, S. Bisson, G. Gerard, L. Becouarn, and E. Lallier. "Mid-infrared generation by difference frequency mixing in orientation-patterned GaAs." *CLEO Conference Paper*, 2001.

32. Liang, Geng-Chiau, Hon-Heuei Liu, A. H. King, A. Mohacsi, A. Miklos, and P. Hess. "Photoacoustic trace detection of methane using compact solid-state lasers," *Journal of Physical Chemistry*, 104, 10179-10183 (16 November 2000).

33. Marple, D. T. F. "Refractive index of GaAs," *Journal of Applied Physics*, 35, 1241-1242 (April 1964).

34. McMullen, J. D. "Optical parametric interactions in isotropic materials using a phase-corrected stack of nonlinear dielectric plates," *Journal of Applied Physics*, 46, 3076-3081 (July 1975).

35. Myers, L. E., R. C. Eckardt, M. M. Fejer, R. L. Byer, W. R. Bosenberg, and J. W. Pierce. "Quasi-phase-matched optical parametric oscillators in bulk periodically poled $LiNbO_3$," *Journal of the Optical Society of America – B*, 12, 2102-2116 (November 1995).

36. Peterson, R. D., K. L. Schepler, J. L. Brown, and P. G. Schunemann. "Damage properties of $ZnGeP_2$ at 2 μm," *Journal of the Optical Society of America – B*," 12, 2142-2146 (November 1995).

37. Piguet, T.J., O. Levi, T. Skauli, L. Eyres, L. Scaccabarozzi, M. M. Fejer, J. S. Harris, T.J. Kulp, S. Bisson, B. Gerard, L. Becouarn, E. Lallier. "Characterization of 0.5mm thick films of orientation-patterned GaAs for nonlinear optical applications," in OSA *Trends in Optics and Photonics (TOPS)Vol. 56, Conference on Lasers and Electro-Optics (CLEO 2001)*, Technical Digest, Postconference Edition. Washington, D.C.: Optical Society of America, 138.

38. -----, Thierry. "Orientation-patterned $Al_xGa_{1-x}As$ for quasiphasematched infrared nonlinear optics." Unpublished PhD defense, Department of Applied Physics, Stanford University, CA, 22 October 2001.

39. Pikhtin, A. N. and A. D. Yas'kov. "Dispersion of the refactive index of semiconductors with diamond and zinc-blende structures," *Soviet Physics – Semiconductors*, 12, 622-626 (June 1978).

40. Powers, P.E., T. J. Kulp and S. E. Bisson. "Continuous tuning of a continuous-wave periodically poled lithium niobate optical parametric oscillator by use of a fan-out grating design," *Optics Letters*, 23, 159-161 (1998).

41. -----, P. E., K. W. Aniolek, T. J. Kulp, B. A. Richman and S. E. Bisson. "Periodically poled lithium niobate optical parametric amplifier seeded with the narrow-band filtered output of an optical parametric generator," *Optics Letters*, 23, 1886-1888 (1998).

42. Richter, Dirk, David G. Lancaster, and Frank K. Tittel. "Development of an automated diode-laser-based multicomponent gas sensor," *Applied Optics*, 39, 4444-4450 (20 August 2000).

43. Roberts, David A. "Simplified characterization of uniaxial and biaxial nonlinear optical crystals: a plea for standardization of nomenclature and conventions," *IEEE Journal of Quantum Electronics*, 28, 2057-2074 (October 1992).

44. Schepler, K. L. Class handouts, OENG 660, Introduction to Nonlinear Optical Devices. School of Engineering and Management, Air Force Institute of Technology, Wright-Patterson AFB OH, January 2001.

45. Schunemann, Peter. "Nonlinear crystals provide high power for the mid-IR," *Laser Focus World*, 85-90 (April 1999).

46. Sell, D. D., H. C. Casey, Jr, and K. W. Wecht. "Concentration dependence of the refractive index for n- and p-type GaAs between 1.2 and 1.8 eV," *Journal of Applied Physics*, 45, 2650-2657 (June 1974).

47. Seraphin, B. O., and Bennet, H. E. in *Semiconductors and semimetals, Volume 3: Optical Properties of III-V Compounds*, Eds. Willardson, R. K. and A. C. Beer. New York: Academic Press, 1967.

48. Szilagyi, A., A. Hordvik, and H. Schlossberg. "A quasi-phase-matching technique for efficient optical mixing and frequency doubling," *Journal of Applied Physics*, 47, 2025-2032 (May 1976).

49. Tanguy, Christian. "Refractive index of direct bandgap semiconductors near the absorption threshold: Influence of exitonic effects," *IEEE Journal of Quantum Electronics*, 32, 1746-1751 (October 1996).

50. Thompson, T. E., J. D. McMullen, and D. B. Anderson. "Second-harmonic generation in GaAs "stack of plates" using high-power CO_2 laser radiation," *Applied Physics Letters*, 29, 113-115 (15 July 1976).

51. Vodopyanov, K. L., J. P. Maffetone, I. Zweiback and W. Ruderman. "$AgGaS_2$ optical parametric oscillator continuously tunable from 3.9 to 11.3 μm," *Applied Physics Letters*, 75, 1204-1206 (30 August 1999).

52. -----, K. L., F. Ganikhanov, J. P. Maffetone, and W. Ruderman. "$ZnGeP_2$ optical parametric oscillator with 3.8-12.4-μm tunability," *Optics Letters*, 25, 841-843 (1 June 2000).

53. Wolfe, William L. and George J. Zissis. *The Inrared Handbook – revised edition*. Washington, D.C.: Office of Naval Research, Department of the Navy, 1993.

54. Yariv, Amnon, Pochi Yeh. *Optical Waves in Crystals – Progagation and Control of Laser Radiation*, New York: Wiley-Interscience, 1984.

55. Zheng, D., L. A. Gordon, Y. S. Wu, R. S. Feigelson, M. M. Fejer, R. L. Byer, and K. L. Vodopyanov. "16-μm infrared generation by difference-frequency mixing in diffusion-bonded-stacked GaAs," *Optics Letters*, 23, (1 July 1998).

56. -----, D., L. A. Gordon, Y. S. Wu, R. K. Route, M. M. Fejer, R. L. Byer, and R. S. Feigleson. “Diffusion bonding of GaAs wafers for nonlinear optics applications,” *Journal of the Electrochemical Society*, 144, 1439-1441 (April 1997).

57. Zeigler, B. C. and K. L. Schepler. “Transmission and damage-threshold measurements in $AgGaSe_2$ at 2.1 μm,” *Applied Optics*, 30, 5077-5080 (1 December 1991).

Vita

Captain Michael D. Harm graduated from King George High School in King George County, Virginia in 1989. He entered undergraduate studies at Virginia Polytechnic Institute and State University (Virginia Tech) in Blacksburg, Virginia, where he graduated with a Bachelor of Science degree in Electrical Engineering in August 1993. He was commissioned through AFROTC Detachment 875 at Virginia Tech.

His first assignment was to the San Antonio Air Logistics Center at Kelly AFB in March of 1994, where he served as an engineer in the Advanced Diagnostic Technology Insertion Center of the Automatic Test Equipment Division. In April of 1995, he was assigned to the 313th Flight Test Squadron at Kelly AFB to serve as a flight test engineer, conducting sustainment-level test and evaluation of improvements to C-5A/B and T-38 aircraft. Captain Harm's next assignment was to the 36th Electronic Warfare Squadron, Eglin AFB, Florida. As an operational test manager for electronic warfare upgrades to ACC aircraft, he organized and conducted numerous tests of upgrades to the F-16 radar warning receiver and chaff and flare dispenser and to other combat aircraft. In August 2000, he entered the Graduate School of Engineering and Management, Air Force Institute of Technology. Upon graduation, he will be assigned to the National Air Intelligence Center at Wright-Patterson AFB, Ohio.

THIS PAGE INTENTIONALLY LEFT BLANK

REPORT DOCUMENTATION PAGE	Form Approved OMB No. 074-0188

1. REPORT DATE *(DD-MM-YYYY)*	2. REPORT TYPE	3. DATES COVERED *(From – To)*
14-03-2002	**Master's Thesis**	Jun 2001 – Mar 2002

4. TITLE AND SUBTITLE

DEVELOPMENT OF A TM:HO:YLF-LASER-PUMPED ORIENTATION-PATTERNED GALLIUM ARSENIDE OPTICAL PARAMETRIC OSCILLATOR

5a. CONTRACT NUMBER

5b. GRANT NUMBER

5c. PROGRAM ELEMENT NUMBER
62204F

6. AUTHOR(S)

Harm, Michael D., Captain, USAF

5d. PROJECT NUMBER

5e. TASK NUMBER

5f. WORK UNIT NUMBER
20010513

7. PERFORMING ORGANIZATION NAMES(S) AND ADDRESS(S)
Air Force Institute of Technology
Graduate School of Engineering and Management (AFIT/EN)
2950 P Street, Building 640
WPAFB OH 45433-7765

8. PERFORMING ORGANIZATION REPORT NUMBER

AFIT/GEO/ENP/02-01

9. SPONSORING/MONITORING AGENCY NAME(S) AND ADDRESS(ES)
AFRL/SNJW
Attn: Mr. Kenneth L. Schepler
3109 P St. DSN: 785-5922 ext274
WPAFB OH 45433-7700 e-mail: Kenneth.Schepler@wpafb.af.mil

10. SPONSOR/MONITOR'S ACRONYM(S)

11. SPONSOR/MONITOR'S REPORT NUMBER(S)

12. DISTRIBUTION/AVAILABILITY STATEMENT

APPROVED FOR PUBLIC RELEASE; DISTRIBUTION UNLIMITED.

13. SUPPLEMENTARY NOTES

14. ABSTRACT

Coherent optical sources in the mid-infrared region (mid-IR) are important fundamental tools for infrared countermeasures and battlefield remote sensing. Nonlinear optical effects can be applied to convert existing near-IR laser sources to radiate in the mid-IR. This research focused on achieving such a conversion with a quasi-phase matched optical parametric oscillators using orientation-patterned gallium arsenide (OPGaAs), a material that can be quasi-phased matched by periodically reversing the crystal structure during the epitaxial growth process. Although non-linear optical conversion was not ultimately achieved during this research, many valuable lessons were learned from working with this material. This thesis reviews the theory of nonlinear optics and explores the importance of accurate refractive index measurements to proper structure design. The details of four nonlinear optical experiments are presented recommendations are offered for the design of future OPGaAs crystals. Recommendations are also made for improved experimental techniques

15. SUBJECT TERMS
gallium arsenide, OPGaAs, quasi-phase matching, orientation-patterned, optical parametric oscillator, OPO, refractive index nonlinear optics, mid-infrared, infrared countermeasures, laser

16. SECURITY CLASSIFICATION OF:			17. LIMITATION OF ABSTRACT	18. NUMBER OF PAGES	19a. NAME OF RESPONSIBLE PERSON
a. REPORT	b. ABSTRACT	c. THIS PAGE			Michael D. Harm, Capt, USAF (ENG)
U	U	U	UU	76	19b. TELEPHONE NUMBER *(Include area code)* (937) 255-6565; e-mail: Michael.Harm@afit.edu

Standard Form 298 (Rev. 8-98)
Prescribed by ANSI Std. Z39-18